BREAKTHROUGH REPORT

Image-based assessment of plant disease progression identifies new genetic loci for resistance

Valérian Méline[a], Denise L. Caldwell[a], Bong-Suk Kim[a], Sriram Baireddy[b], Changye Yang[b], Erin E. Sparks[c], Edward J. Delp[b], and Anjali S. Iyer-Pascuzzi[a†]

[a] 915 W. State Street, Department of Botany and Plant Pathology, Purdue University, West Lafayette, Indiana, USA

[b] Video and Image Processing Laboratory (VIPER), School of Electrical and Computer Engineering

[c] Department of Plant and Soil Sciences and the Delaware Biotechnology Institute, University of Delaware, Newark, DE

†Author for correspondence: asi2@purdue.edu

Keywords: Digital phenotyping, QTL, *Ralstonia*, bacterial wilt, tomato

Short title: Disease resistance QTL and image-based phenotyping

Material distribution: The author(s) responsible for distribution of materials integral to the findings presented in this article in accordance with the policy described in the Instructions for Authors (https://academic.oup.com/plcell/pages/General-Instructions) are: Anjali Iyer-Pascuzzi (asi2@purdue.edu) and Edward J. Delp (ace@purdue.edu).

Abstract

A major challenge in global crop production is mitigating yield loss due to plant diseases. One of the best means of disease control is plant resistance, but the identification of genes that promote resistance has been limited by the subjective quantification of disease, which is typically scored by the human eye. We hypothesized that image-based, non-destructive quantification of disease phenotypes would enable the rapid identification of new disease resistance loci. We tested this using the interaction between tomato and *Ralstonia solanacearum*, a soilborne pathogen that causes bacterial wilt disease. We acquired over 40,000 time-series images of disease progression in a tomato recombinant inbred line population, and developed an image analysis pipeline providing a suite of ten traits to quantify wilt disease based on plant shape and size. Quantitative trait loci (QTL) analyses using image-based phenotyping identified QTL that were both unique and shared compared with those identified by human assessment of wilting. When shared loci were identified, image-based phenotyping could detect some QTL several days earlier than human assessment. Thus, expanding the phenotypic space of disease with image-based, non-destructive phenotyping allowed both earlier detection and identified new genetic components of resistance.

Introduction

Plant diseases are a significant global constraint to crop production. Developing disease resistant crops requires identifying the plant genomic regions and genes that contribute to resistance to the pathogenic microbes that cause disease. This in turn depends on phenotyping large populations of plants for their responses to pathogens. Phenotyping plant diseases is challenging because diseases cause complex, quantitative phenotypes that can occur at different scales – e.g. on parts of leaves, entire leaves, or the whole plant. In addition, disease phenotypes vary over time and depend on environmental conditions, plant age, and pathogen virulence. Disease symptoms such as wilting or necrotic spots have traditionally been scored with the human eye, but these scores are subjective, can vary by individual, and are difficulty to accurately quantify.

The challenging nature of visual disease assessment has led to the use of sensors including RGB, hyperspectral, chlorophyll fluorescence and thermal cameras to assess disease symptoms (Colwell, 1956; Jackson, 1986; Bock et al., 2010; Simko et al., 2017). Compared to assessment by the human eye, image-based phenotyping is faster, more reproducible, and more sensitive to small variations in disease symptoms that can be critical for detecting resistance loci (Bock et al., 2008, 2010; Stewart and McDonald, 2014; Stewart et al., 2016; Simko et al., 2017; Shakoor et al., 2017). Many studies have used or developed tools to assess plant symptoms using different types of sensors (Mahlein, 2016; Mahlein et al., 2017, 2019; Lowe et al., 2017; Shakoor et al., 2017; Mochida et al., 2019; Mir et al., 2019; Pérez-Bueno et al., 2019; Pineda et al., 2021; Simko et al., 2017). However, few studies have used these technologies in QTL or Genome Wide Association (GWA) analyses for responses to plant pathogens, and all have used destructive methods (Yates et al., 2019; Fordyce et al., 2018; Corwin et al., 2016). It has remained challenging to use image-based, non-destructive phenotyping for disease resistance across large populations, both because of technical factors like the expense of phenotyping platforms and the time associated with imaging, and also biological factors such as differences in plant morphology and disease progression within a population.

The soil-borne betaproteobacterium *Ralstonia solanacearum* is the causal agent of bacterial wilt disease and has been ranked as one of the top 10 most destructive plant bacterial pathogens of all time (Mansfield et al., 2012). *Ralstonia* infection causes susceptible plants to wilt, and the

amount of wilting correlates with a plant's level of susceptibility (Genin, 2010; Genin and Denny, 2011). The bacterium is a major production constraint in Solanaceous crops both globally and in the United States, where disease loss in tomatoes can exceed 70%. In crops, resistance to *Ralstonia* is quantitative, but the quantitative trait loci (QTL) underlying resistance to US strains of *Ralstonia* are largely unknown. QTL for other strains have been mapped (Danesh et al., 1994; Thoquet et al., 1996a, 1996b; Mangin et al., 1999; Wang et al., 2000; Carmeille et al., 2006; Jaw-Fen Wang et al., 2013; Shin et al., 2020) but have not been cloned, and the host determinants necessary for resistance remain mostly unspecified.

The limited identification of QTL for *Ralstonia* resistance can be attributed in part to the difficulty in accurately scoring plant wilting. Wilting is traditionally measured on a 0 – 4 scale, in which 0 indicates a plant with no wilting, 1 = 1 – 25%, 2 = 26 – 50%, 3 = 51 – 75% and a score of 4 indicates a plant with 76 – 100% wilted leaves (Schandry, 2017). While it is straightforward to assess the ends of the spectrum, rating plants with scores of 2 or 3 is particularly difficult. This is due to the subjective nature of visually determining when a leaf has lost sufficient turgor to qualify as wilted. Reliable disease phenotyping is critical for identifying QTL for resistance to *Ralstonia* and the development of resistant varieties.

Here, we used image-based, rapid, non-destructive phenotyping to identify new tomato genetic resistance loci to *Ralstonia*. We developed a rapid, semi-automated imaging and trait analysis pipeline to quantify bacterial wilt disease in a recombinant inbred line (RIL) population derived from *Ralstonia*-resistant and susceptible tomato genotypes. We found both unique and shared QTL between our image-based traits and plant wilting scored by the human eye. At least one of the QTL was detected by image-based phenotyping before the onset of visual symptoms, demonstrating that image-based phenotyping captures the disease phenotype at early stages of infection. These results demonstrate that imaged-based, non-destructive phenotyping can shed light on new aspects of disease and improve our ability to identify genetic loci crop resistance.

Results

Development of an aboveground imaging and semi-automated analysis pipeline

80 We first constructed a simple, low-cost imaging system that allowed us to semi-automate
81 aboveground disease phenotyping. Each plant was placed on a commercially available turntable,
82 and plants were imaged with a Canon DSLR (Supplemental Figure 1; details in methods). The
83 turntable and camera were connected with Photocapture 360 (Ortery technologies), which
84 allowed us to automatically capture images every 45 degrees (8 images per plant). Using this
85 system, we were able to non-destructively image each plant in less than 2 minutes, with minimal
86 manual labor. Each image included a fiducial marker for post-image color correction. Plants in
87 the F_9 generation from a RIL population derived from a cross between resistant Hawaii 7996
88 (H7996) and susceptible West Virginia 700 (WV) were imaged the day before inoculation with
89 *R. solanacearum* strain K60, and at 3, 4, 5 and 6 days post inoculation (dpi). At 3 dpi, symptoms
90 were not present in susceptible parent WV, but by 6 dpi these plants were completely wilted. We
91 imaged five replicate plants of each RIL as well as the parental lines. Using this system, we
92 captured over 40,000 images for high-resolution disease phenotyping. The same set of plants was
93 also visually scored by the human eye at 8 dpi. Visual scoring was based on the percentage of
94 wilted leaves. Tomato phenotypes in the RIL population ranged from highly susceptible to
95 highly resistant, consistent with the quantitative nature of disease resistance (Supplemental
96 Figures 2 and 3).
97
98 We next developed a set of mathematical descriptors to phenotype wilting over time in our
99 images. Plant wilting is a composite phenotype, and we used 10 image-based traits
100 (Supplemental Table 1) to describe different aspects of wilting: convex area, convex width, plant
101 area, plant height, plant width, X mass, Y mass, center of mass (CM) height, CM width, and
102 color. Several of these, such as the area and width of the convex hull, are traditional methods of
103 describing aboveground plant shape. Because the center of mass of a plant leaf changes as a
104 plant wilts, we developed additional descriptors based on the distance of the leaf center of mass
105 from the stem (CM width and CM height, X mass and Y mass). We then developed a pipeline
106 which used the original image as input, performed color correction, and quantified each
107 descriptor (Figure 1 and Supplemental Figure 4, and methods).
108
109
110

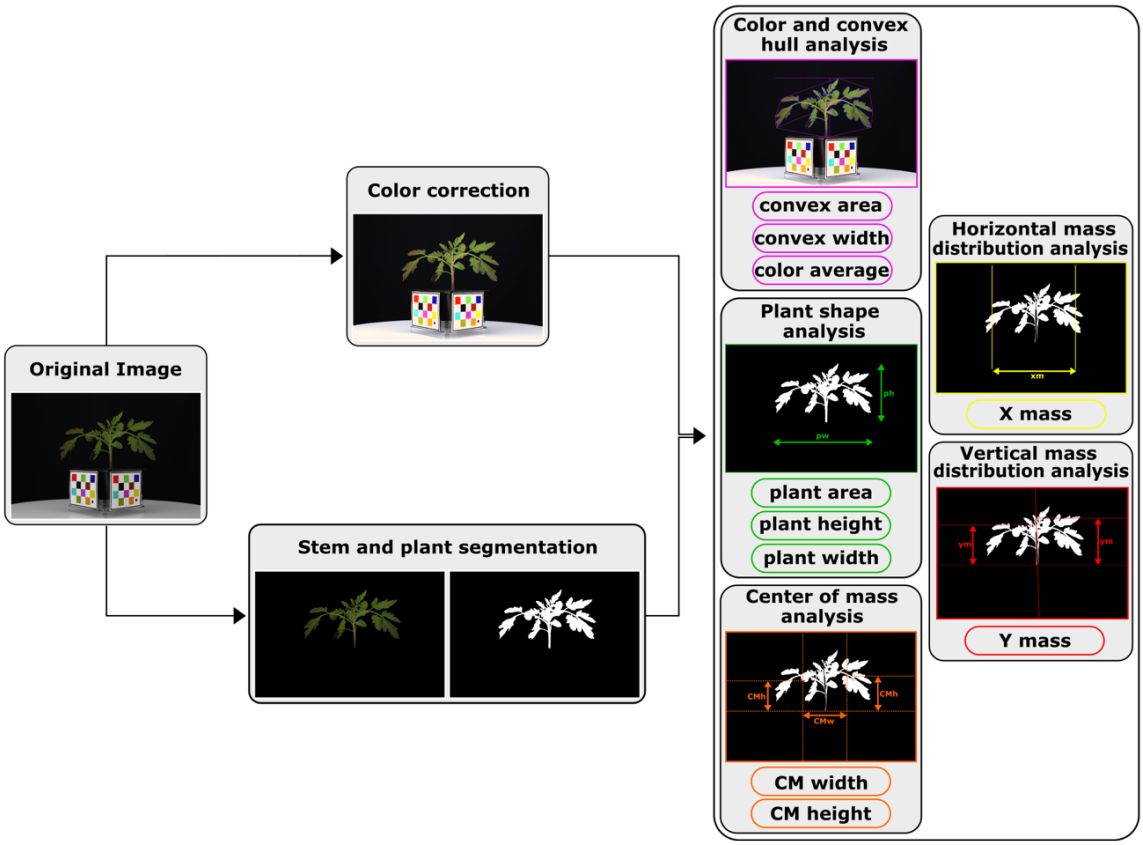

Figure 1: Diagram of the semi-automated analysis pipeline and 10 image descriptors

Image-based traits differentiate resistant and susceptible plants

To validate the efficiency of the image-based descriptors to estimate wilting phenotypes, we tested whether image-based phenotyping descriptors could differentiate resistant from susceptible plants. Supplemental Figure 5 shows the average normalized score for each of the image-based descriptors for each parent and the RIL population from -1 (the day before inoculation) to 6 dpi. Most descriptors, particularly those based on plant width or convex hull, had clearly divergent values in resistant and susceptible plants at a given time point. RIL descriptor values ranged from those of the resistant to susceptible parents and occasionally showed transgressive segregation (Supplemental Figure 5). Because plant shape at 6 dpi depends on shape of the same plant at -1 dpi, we used the evolution of each descriptor from day -1 to 6 dpi in our QTL analysis. This evolution was termed a 'trait'. Trait values were clearly different for resistant and susceptible parents for all traits except color (Figure 2), which was not used further.

a.

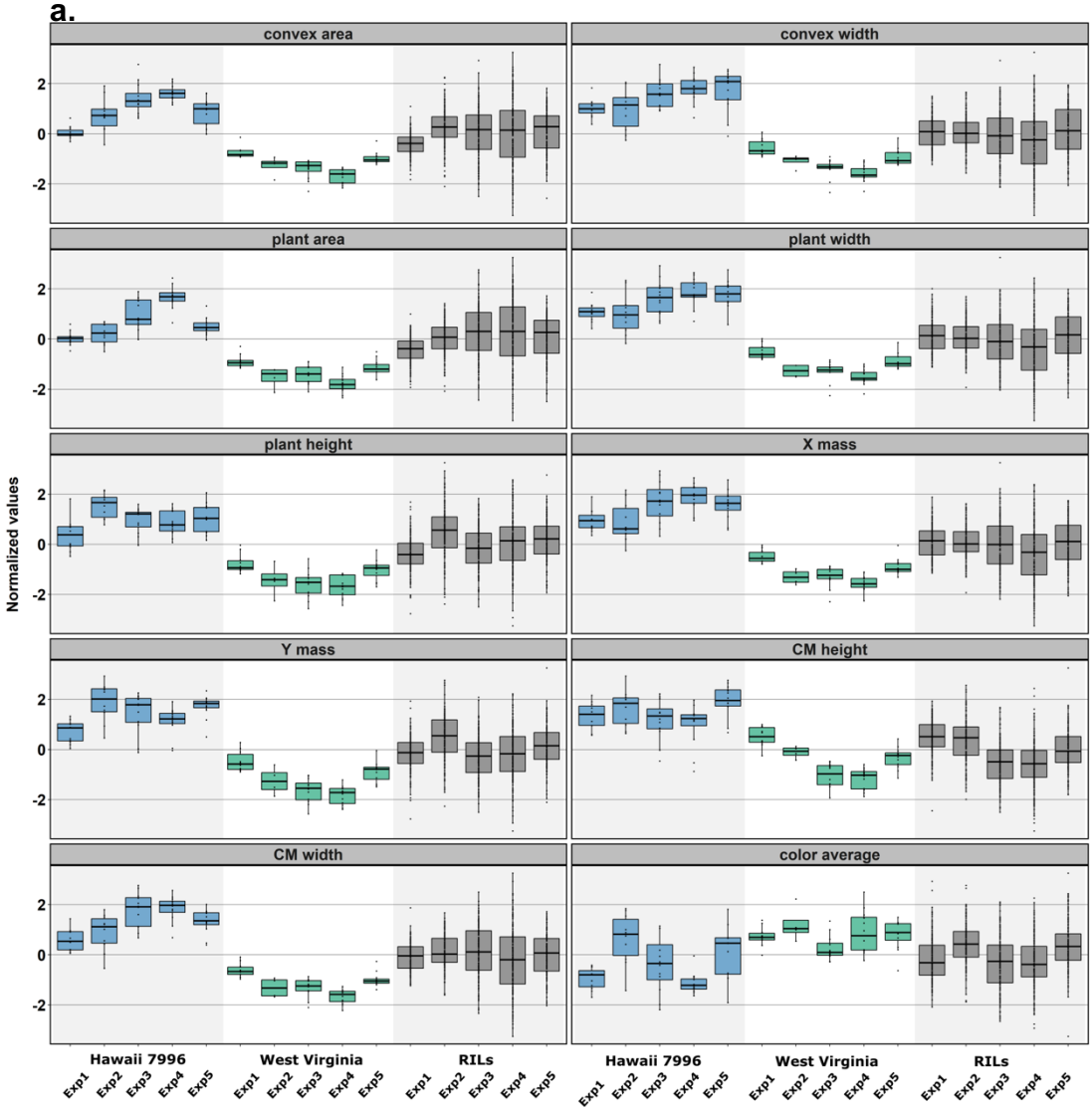
convex area
convex width
plant area
plant width
plant height
X mass
Y mass
CM height
CM width
color average
Normalized values
2
0
-2
Hawaii 7996
West Virginia
RILs
Exp1
Exp2
Exp3
Exp4
Exp5

b.

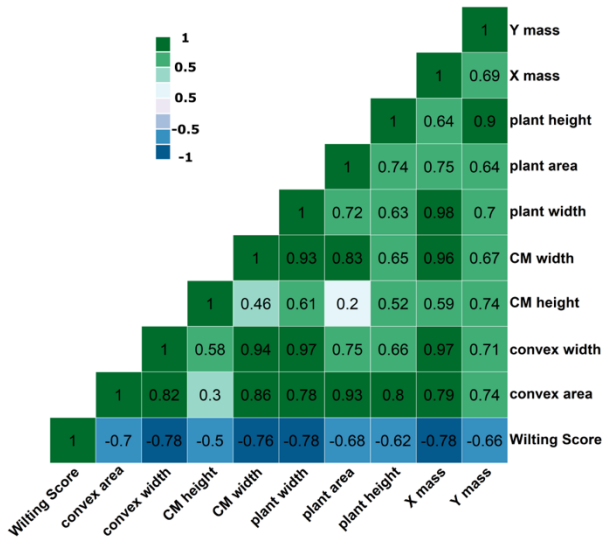
1
0.5
0.5
-0.5
-1
Y mass
X mass
plant height
plant area
plant width
CM width
CM height
convex width
convex area
Wilting Score
1
1 0.69
1 0.64 0.9
1 0.74 0.75 0.64
1 0.72 0.63 0.98 0.7
1 0.93 0.83 0.65 0.96 0.67
1 0.46 0.61 0.2 0.52 0.59 0.74
1 0.58 0.94 0.97 0.75 0.66 0.97 0.71
1 0.82 0.3 0.86 0.78 0.93 0.8 0.79 0.74
1 -0.7 -0.78 -0.5 -0.76 -0.78 -0.68 -0.62 -0.78 -0.66

126

Figure 2: Trait evolution during disease and correlation among descriptors. a. Boxplots showing the evolution of the normalized values between -1 and 6 dpi for each of the five biological replicates for the ten image-based traits for resistant Hawaii 7996, susceptible West Virginia parents and the 166 RILs. Color was unable to differentiate resistant from susceptible plants and was not used further. b. Heatmap showing the Pearson correlation values between image-based traits used in our QTL analysis and the human eye based wilting score in 2019. The correlations values were determined using the same plants imaged and visually assessed in 2019.

Image-based phenotyping reveals drivers of the wilting phenotype

We next investigated whether any of our traits were major components of the wilting phenotype. We visually scored plants and asked how well our image-based traits correlated with human visual scoring. Wilting is categorized by loss of plant leaf turgor that results in drooping leaves, and decreased plant width and height. Determining how much a plant has wilted is challenging, in part because it can be difficult to quantify how much each a leaf has drooped and how much drooping of one leaf correlates with whole plant wilting.

We aimed to quantify leaf drooping using center of mass traits. Among our image-based traits, those which were functions of the leaf center of mass were highly inversely correlated with visual wilting (i.e. as a plant wilts, the center of mass decreases), suggesting that these are major drivers of the wilting phenotype. These traits included CM width, plant width and X mass ($r > -0.75$) (Figure 2B).

Several of our traits describe similar aspects of plant shape, such as height or width, through different methods. These traits tended to be highly correlated with each other. For example, plant height vs Y mass use different methods to describe plant width (based on the plant mask or the center of mass of the stem masks; see Methods), and were highly positively correlated with each other (0.93; Figure 2B).

151 We trained a random forest, consisting of 1000 decision trees, to use data from 6 dpi to predict
152 the expert visual score assigned at 8 dpi. We used 969 plants in a 60:40 training-testing data
153 split, and achieved a classification accuracy of 83%. To identify the traits that provided the most
154 efficient estimation of wilting symptoms, we randomly scrambled the nine image-based traits
155 one at a time. Plant width and plant area had the most impact on wilting score prediction
156 (Supplemental Figure 6).
157
158 *QTL analysis identifies 20 wilting QTL in 10 clusters across the tomato genome at 6 dpi*
159 Our overall goal was to identify tomato genomic regions that provide resistance or susceptibility
160 to *Ralstonia*. Prior to this analysis, we first generated a genetic map using Genotyping-by-
161 Sequencing (GBS). We identified 632 high-quality SNPs for linkage mapping using GBS. We
162 combined these with 112 SolCap markers, and subsequently generated a linkage map using ICI
163 mapping software (Meng et al., 2015). Our linkage map consisted of ~1300 cM (Supplemental
164 Figure 7) with an average per chromosome marker density that varies from 1.8 to 7.48 cM
165 (Supplemental Table 2).
166
167 For QTL analysis, we mapped the evolution of each our nine image-based descriptors from -1 to
168 6 dpi. In addition to the image-based phenotyping, we used two years (2016 and 2019) of
169 visually scored phenotyping data at 8 dpi. Visually assessed wilt scores from 2019 were
170 quantified from the same plants that were used for image-based phenotyping. In 2016, plants
171 were only visually scored for wilting, and no image-based measurements were taken. Using ICI
172 mapping software and composite interval mapping (CIM) for all traits, we identified 20 QTL
173 within the RIL population with a LOD score above 3 (Table 1). To be consistent with previous
174 studies of tomato-*Ralstonia* QTL mapping, we call these QTL, 'Bacterial wilt resistance (*Bwr*)
175 QTL'. Each *Bwr* QTL explained approximately 6 to 11% of the variation in response to *R.*
176 *solanacearum* strain K60, and together the clusters explained more than 88% of the variation
177 (calculated using the sum of the QTL with the highest PVE in each cluster).
178
179 The parent that donated the favorable allele was determined according to the sign of the QTL
180 additive effect (Awata et al., 2020), where a positive sign referred to H7996 resistant parent and
181 a negative sign to WV susceptible parent. Typically, in QTL analysis, the favorable allele has the

Chromosome	Cluster	Position	LeftMarker	RightMarker	TraitName	LOD	PVE	Add	LeftCI	RightCI
2	Bwr2.1	45	solcap_snp_sl_18519	SL3.0ch02-49265134	plant width	3.4108	6.4576	-0.1669	42.5	47.5
2	Bwr2.2	72	SL3.0ch02-45885016	SL3.0ch02-44375028	X mass	3.4765	9.4924	-0.2178	69.5	73.5
2	Bwr2.2	72	SL3.0ch02-45885016	SL3.0ch02-44375028	CM width	3.2455	8.455	-0.2189	69.5	73.5
3	Bwr3.1	22	solcap_snp_sl_14355	solcap_snp_sl_9689	convex width	5.3238	10.2506	0.2103	21.5	26.5
3	Bwr3.1	22	solcap_snp_sl_14355	solcap_snp_sl_9689	plant width	4.7309	9.1511	0.1976	21.5	25.5
3	Bwr3.1	22	solcap_snp_sl_14355	solcap_snp_sl_9689	X mass	3.4765	5.8012	0.1705	21.5	26.5
3	Bwr3.1	23	solcap_snp_sl_14355	solcap_snp_sl_9689	CM width	3.6627	6.2716	0.1887	21.5	27.5
3	Bwr3.1	25	solcap_snp_sl_14355	solcap_snp_sl_9689	plant height	4.5107	7.6902	0.1896	21.5	31.5
3	Bwr3.1	25	solcap_snp_sl_14355	solcap_snp_sl_9689	Y mass	3.3918	9.3283	0.1708	21.5	31.5
3	Bwr3.2	38	solcap_snp_sl_21215	solcap_snp_sl_9663	Wilting Score 2016	3.5258	7.3736	-0.1726	35.5	39.5
3	Bwr3.2	38	solcap_snp_sl_21215	solcap_snp_sl_9663	convex area	3.4328	9.0796	0.1953	34.5	39.5
3	Bwr3.2	38	solcap_snp_sl_21215	solcap_snp_sl_9663	plant area	3.3019	8.6697	0.1902	34.5	39.5
4	Bwr4.1	4	SL3.0ch04-60431371	solcap_snp_sl_11543	convex width	3.1855	6.0199	0.1627	1.5	10.5
5	Bwr5.1	100	solcap_snp_sl_22649	SL3.0ch05-65105663	plant height	3.6115	9.4852	0.2103	95.5	103.5
6	Bwr6.1	79	solcap_snp_sl_14458	SL3.0ch06-39435402	Wilting Score 2016	4.077	8.7626	-0.1871	76.5	81.5
6	Bwr6.1	81	solcap_snp_sl_14458	SL3.0ch06-39435402	Wilting Score 2019	3.2673	11.0473	-0.1621	78.5	81.5
10	Bwr10.1	53	solcap_snp_sl_33168	SL3.0ch10-63377492	plant width	3.8661	7.6897	-0.1811	50.5	54.5
10	Bwr10.1	53	solcap_snp_sl_33168	SL3.0ch10-63377492	convex width	3.4883	6.8155	-0.1714	50.5	54.5
12	Bwr12.1	37	solcap_snp_sl_1525	solcap_snp_sl_1572	CM height	4.1755	10.7222	0.1837	33.5	40.5
12	Bwr12.2	42	solcap_snp_sl_58807	solcap_snp_sl_9707	Y mass	3.3249	8.5939	0.1651	40.5	43.5

Table 1 Overview of the 20 wilting QTL identified in 10 clusters across the tomato genome at 6 dpi. LOD: maximum value of the Logarithm of the odd. PVE: Percentage of phenotypic variance explained. Add: Additive effect. Left CI and Right CI are the confidence interval calculated by a one-LOD decrease from the estimated QTL position.

182 higher trait value. Here, a higher trait value is favorable in all cases except the visual wilting
183 score, in which a higher trait value was associated with susceptibility (e.g. 90% wilting is more
184 susceptible than 20% wilting). For QTL detected using our visual wilting score, the susceptibility
185 allele was contributed by the susceptible parent WV (Table 1), consistent with other tomato-*R.*
186 *solanacearum* QTL studies based on visual assessment of wilting. For all QTL except those on
187 chromosome 2 and 10, the favorable allele was contributed by Hawaii 7996. QTL clusters on
188 chromosome 2 and 10, which contributed to plant height and width, were donated by the
189 susceptible parent WV. Favorable allelic contribution from both resistant and susceptible parents
190 is common in QTL studies for resistance (Maschietto et al., 2017; Awata et al., 2020).
191
192 Among the 20 individual *Bwr* QTL were 10 QTL clusters (Table 1). We use the term 'QTL
193 cluster' to describe QTL for different traits that co-localize at the same left and right genetic

194 marker. There are between one and six *Bwr* QTL within a given cluster, and each QTL within
195 the cluster has different LOD scores and explains a different percentage of phenotypic variation.
196 *Bwr* QTL for traits that are highly correlated with each other (Figure 2B) tended to cluster
197 together. For example, a cluster of QTL on chromosome 3 (*Bwr3.1*; Table 1) contains six *Bwr*
198 QTL, including three for area-related traits (convex width, and X mass and CM width), which
199 are correlated with each other at r = 0.94 - 0.97 (Figure 2B). In another cluster (*Bwr3.2*) on this
200 same chromosome, *Bwr* QTL for traits that describe plant area were detected together. This co-
201 localization supports the robust nature of our analyses.
202
203 In other clusters, only one trait that described one aspect of the wilting phenotype was present.
204 For example, despite several metrics that describe width, only convex width was identified as a
205 QTL on chromosome 4 (*Bwr4.1*; LOD 3.18; PVE = 6%). This suggests that the image-based
206 phenotyping captured genetic variation that is specific to each trait.
207
208 *Image-based non-destructive phenotyping identifies three types of QTL clusters*
209 Among our *Bwr* QTL clusters, we identified three types: those found using both image-based
210 and visual phenotyping (1 cluster, *Bwr3.2*), those found only through visual phenotyping (1
211 cluster, *Bwr6.1*), and those that were identified only through image-based phenotyping (8
212 clusters; Table 1 and Figure 3).
213
214 For the cluster including both image-based and visual phenotyping, (*Bwr3.2*) on chromosome 3,
215 we detected QTL for convex area, plant area and visual plant wilting in 2016 (Table 1 and Figure
216 3a). Previous studies examining tomato responses to other strains of *Ralstonia* have not detected
217 *Bwr* QTL in this region, indicating that it may be a novel target for *R. solanacearum* strain K60.
218 The identification of both image-based and visual QTL within the same cluster suggests that our
219 phenotyping methods are robust at identifying features of plant wilting. Close to this cluster is
220 *Bwr3.1*, which detected QTL for traits based on plant width, including convex width and CM
221 width. The proximal arm of chromosome 3 may be an important but unexploited region for
222 defense against *R. solanacearum* strain K60.

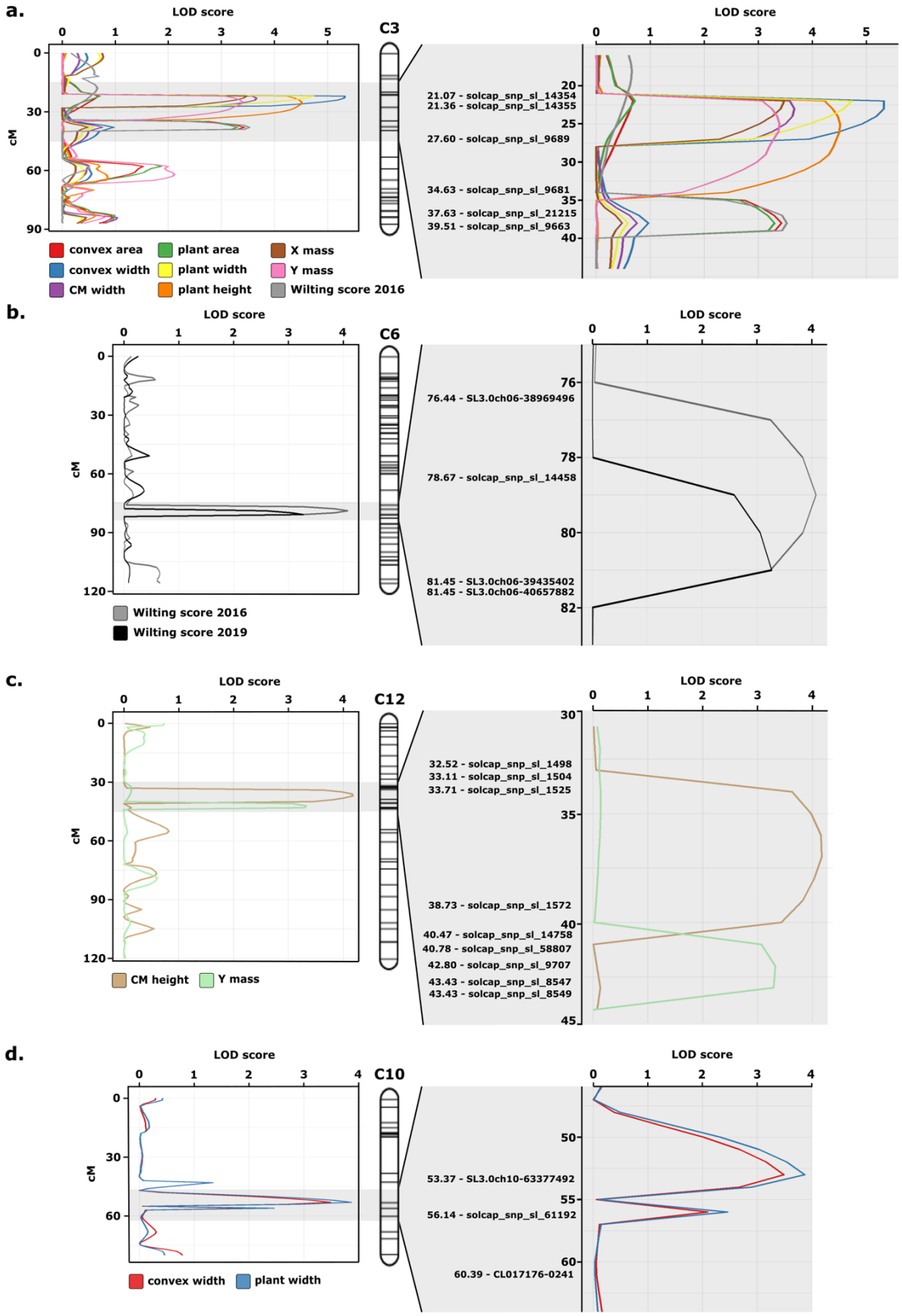
a.
LOD score
C3
cM
convex area
convex width
CM width
plant area
plant width
plant height
X mass
Y mass
Wilting score 2016
21.07 - solcap_snp_sl_14354
21.36 - solcap_snp_sl_14355
27.60 - solcap_snp_sl_9689
34.63 - solcap_snp_sl_9681
37.63 - solcap_snp_sl_21215
39.51 - solcap_snp_sl_9663
b.
C6
Wilting score 2016
Wilting score 2019
76.44 - SL3.0ch06-38969496
78.67 - solcap_snp_sl_14458
81.45 - SL3.0ch06-39435402
81.45 - SL3.0ch06-40657882
c.
C12
CM height
Y mass
32.52 - solcap_snp_sl_1498
33.11 - solcap_snp_sl_1504
33.71 - solcap_snp_sl_1525
38.73 - solcap_snp_sl_1572
40.47 - solcap_snp_sl_14758
40.78 - solcap_snp_sl_58807
42.80 - solcap_snp_sl_9707
43.43 - solcap_snp_sl_8547
43.43 - solcap_snp_sl_8549
d.
C10
convex width
plant width
53.37 - SL3.0ch10-63377492
56.14 - solcap_snp_sl_61192
60.39 - CL017176-0241

223

Figure 3: Significant QTL clusters on chromosomes 3 (a.), 6 (b.), 12 (c.) and 10 (d.). The image-based and visually assessed traits are represented with different colors for each chromosome. The vertical axis represents the genetic position (cM) and horizontal axis shows the LOD score. For each chromosome, the left panel represents the entire chromosome and the right panel represents the significant QTL cluster regions.

224

225 On chromosome 6 we detected *Bwr* (*Bwr6.1*) using only visual assessment for both 2016 and
226 2019 (Table 1, Figure 3b). This region may be a 'hot spot' for QTL for resistance to multiple
227 strains of *Ralstonia*. Previous studies using this same tomato population for mapping *Bwr* to
228 other strains of *Ralstonia* detected QTL approximately 4 Mb from this position (Supplemental
229 Figure 7).

230

231 In all other clusters, QTL were identified using only image-based phenotyping. Two such
232 clusters, detected on chromosome 12, identified QTL for CM height (*Bwr12.1*) and Y mass
233 (*Bwr12.2*), and were located near previous QTL detected against other strains of *Ralstonia*
234 (Supplemental Figure 7 and Figure 3c) . These previous studies (Wang et al., 2000; Jaw-Fen
235 Wang et al., 2013; Shin et al., 2020) detected QTL using visual wilt assessment of adult plants in
236 the field.

237

238 The remaining QTL detected through image-based phenotyping have not been previously
239 identified in studies using other strains of *Ralstonia*. These regions may be effective only against
240 specific strains of *Ralstonia* ('strain-specific' QTL), or may include those that are not easily
241 detected using visual assessment. In support of the latter, at one of the image-based-only clusters,
242 *Bwr10.1* (Figure 3d), we detected a QTL using visual assessment that did not meet our threshold
243 for significance after permutation (Supplemental Table 3). Thus, image-based phenotyping
244 improved our ability to detect QTL.

245

246 *Image-based phenotyping identified Bwr QTL prior to visual symptom development*
247 In our system, wilting symptoms begin to appear on highly susceptible plants at 4 dpi, and these
248 plants are nearly 100% wilted by 6 dpi. To test whether we could detect *Bwr* QTL prior to the
249 onset of visual symptoms, we performed QTL analysis at 3, 4 and 5 dpi. No QTL were identified
250 based on visual assessment at any of these time points, however several QTL were identified
251 based on image-based phenotyping. At 3 dpi, three clusters were detected on chromosome 3, two

252 of which co-localized with those identified at 6 dpi (Supplemental Table 4). *Bwr3.1*, a cluster
253 detected only by image-based phenotyping, and *Bwr3.2*, a cluster detected by both visual and
254 image-based phenotyping, were first detected at 3 dpi. *Bwr3.1* was also detected at 5 and 6 dpi,
255 while *Bwr3.2* was detected 3, 4, 5 and 6 dpi (Supplemental Table 4). A small number of
256 additional QTL were detected at earlier time points (Supplemental Table 4), but in most cases
257 these were not stable, since they were not present at 6 dpi. These data suggest that image-based
258 phenotyping can identify *Bwr* QTL prior to the onset of wilting symptoms.
259
260 *Plant architecture QTL do not overlap with Bwr QTL*
261 The parents of the RIL population, H7996 and WV, have different aboveground phenotypes
262 (Supplemental Figure 4) and the shoot architecture of the RILs correspondingly varies. To ensure
263 that *Bwr* QTL were the result of tomato responses to *Ralstonia*, and not due to differences in
264 aboveground plant architecture, we used our traits in a QTL analysis at -1 dpi, the day before
265 plants had been inoculated. We call these 'tomato plant architecture (*Tpa*)' QTL. We identified
266 16 *Tpa*, within 9 QTL clusters (Table 2). None of the 16 *Tpa* were detected within the same
267 interval as *Bwr* at 6 dpi. However, two *Tpa* QTL clusters were detected that were near *Bwr* QTL
268 present at 6 dpi. One of these was detected on chromosome 3 at position 30, between *Bwr3.1*
269 and *3.2*.

Chromosome	Cluster	Position	LeftMarker	RightMarker	TraitName	LOD	PVE	Add	LeftCI
2	Tpa2.1	117	solcap_snp_sl_8510	solcap_snp_sl_15574	plant width	3.3851	6.4842	0.129	114.5
2	Tpa2.1	117	solcap_snp_sl_8510	solcap_snp_sl_15574	X mass	4.1424	6.8279	0.139	114.5
3	Tpa3.1	30	solcap_snp_sl_9689	solcap_snp_sl_9681	plant area	3.6327	8.0934	0.1522	24.5
3	Tpa3.2	58	SL3.0ch03-61078160	solcap_snp_sl_10372	plant width	3.2538	9.4831	0.1555	56.5
3	Tpa3.2	58	SL3.0ch03-61078160	solcap_snp_sl_10372	X mass	3.8291	9.4218	0.1628	56.5
3	Tpa3.2	59	SL3.0ch03-61078160	solcap_snp_sl_10372	CM height	3.794	3.6957	0.1603	56.5
4	Tpa4.1	128	SL3.0ch04-1213025	solcap_snp_sl_63869	CM height	3.8063	12.0286	-0.2891	127.5
6	Tpa6.1	10	SL3.0ch06-13533085	SL3.0ch06-3310762	convex area	4.741	11.2755	0.1621	8.5
6	Tpa6.1	10	SL3.0ch06-13533085	SL3.0ch06-3310762	plant width	3.5865	6.9265	0.1336	8.5
6	Tpa6.1	10	SL3.0ch06-13533085	SL3.0ch06-3310762	plant area	3.5117	7.3344	0.1457	8.5
6	Tpa6.1	10	SL3.0ch06-13533085	SL3.0ch06-3310762	X mass	4.8686	8.016	0.151	8.5
6	Tpa6.1	10	SL3.0ch06-13533085	SL3.0ch06-3310762	Y mass	4.902	9.3612	0.1757	8.5
8	Tpa8.1	80	solcap_snp_sl_21461	SL3.0ch08-63373341	X mass	3.2439	5.3622	0.123	74.5
9	Tpa9.1	36	solcap_snp_sl_26683	SL3.0ch09-4516570	CM height	4.8307	6.146	0.2081	32.5
9	Tpa9.2	67	SL3.0ch09-39293163	SL3.0ch09-63338944	convex area	3.1976	7.523	-0.1323	60.5
10	Tpa10.1	71	solcap_snp_sl_8835	Le013158s_161	Y mass	3.2077	5.9734	0.1404	68.5

Table 2 Overview of tomato plant architecture (Tpa) QTL identified at -1 dpi by image-based phenotyping.

While we cannot rule out the possibility that the same genes underlie these *Tpa* and *Bwr* QTL, their different marker intervals, coupled with the visual wilting QTL that is within the *Bwr3.2* cluster, suggests that different genes are responsible for these QTL. Together, these data suggest that our image-based phenotyping detected genomic regions that function in responding to *Ralstonia* and *Bwr* QTL are not the result of differential growth patterns within the RILs.

Discussion

Breeding for plant disease resistance is one of the best strategies to combat plant diseases and prevent major crop loss, but is challenging in part due to the complicated nature of disease phenotyping. Here we used rapid, non-destructive, image-based phenotyping with RGB images to identify 20 QTL in 10 clusters for tomato responses to *Ralstonia* at 6 dpi, two of which were detected as early as 3 dpi. Together, the 20 *Bwr* QTL at 6 dpi explained more than 88% of the variation in response to *Ralstonia*. Image-based phenotyping for shape-based traits that were correlated with wilting detected both novel loci and those that overlapped with QTL based on human visual assessment. These results establish the importance and feasibility of quantitative, non-destructive, imaged-based phenotyping to identify new genetic targets for crop disease resistance during disease progression.

Benefits of image-based phenotyping

Imaged-based phenotyping has been used to detect QTL associated with plant root (Topp et al., 2013) and shoot (Zhang et al., 2017; Knoch et al., 2020; Li et al., 2020) architecture, plant height (Wang et al., 2019), salt stress (Awlia et al.), and yield (Tanger et al., 2017; Pauli et al., 2016) among other traits. Although image-based phenotyping has become increasingly common to quantify plant disease symptoms (Mahlein, 2016; Mahlein et al., 2017, 2019; Lowe et al., 2017; Shakoor et al., 2017; Mochida et al., 2019; Mir et al., 2019; Pérez-Bueno et al., 2019; Pineda et al., 2021; Simko et al., 2017), few studies have used this technology to identify new genetic loci for plant disease resistance (Yates et al., 2019; Fordyce et al., 2018; Corwin et al., 2016). One reason for this may be that many plant disease symptoms occur at the leaf scale (such as spots and specks), making it difficult to use some sensors non-destructively and in high-throughput, or at the proper resolution needed to assess disease. For example, automated digital phenotyping of

301 Septoria Tritici Blotch on wheat leaves identified novel QTL for resistance, but the destructive
302 phenotyping required significant manual labor to harvest, mount and scan leaves (Yates et al.,
303 2019). While wilting does occur at the leaf scale, it is an easier phenotype to assess at the whole
304 plant scale. Another possibility is that imaging sensors are often expensive, making it more
305 challenging to phenotype the large number of plants needed in a QTL or GWA study. Our
306 method is low-cost and rapid (< 2 min/plant), and requires no manual labor other than placing
307 the plant on the turntable and initiating imaging via a computer.
308
309 Our image-based phenotyping identified loci that function in tomato responses to *Ralstonia*, but
310 did not detect one of the two *Bwr* clusters (*Bwr6.1*) we found using visual assessment of disease.
311 Visual assessment was performed at 8 dpi, while our image based phenotyping ended at 6 dpi. It
312 is possible *Bwr6.1* is not apparent until very late stages of disease. Alternatively, these results
313 could mean that we missed components of wilting in our image-based traits. However, a more
314 likely explanation is that our image-based traits were averaged across eight two dimensional
315 images, but wilting is a three dimensional (3D) phenotype. Images in 3D may allow detection of
316 *Bwr6.1*. It would also be of interest to test whether using additional types of sensors, such as
317 hyperspectral, would identify *Bwr 6.1*. Multi and hyperspectral imaging has been used to detect
318 biochemical changes in disease (Mahlein et al., 2017; Lowe et al., 2017; Zhang et al., 2020).
319 Given the chemical changes that occur during water stress, this type of imaging would likely
320 identify additional genetic variation associated with resistance to bacterial wilt disease.
321
322 *New QTL for responses to Ralstonia in tomato*
323 As in tomato, resistance to *Ralstonia* in other Solanaceous crops is quantitative (Young and
324 Danesh, 1994; Danesh et al., 1994; Thoquet et al., 1996a, 1996b; Mangin et al., 1999; Wang et
325 al., 2000; Carmeille et al., 2006; Jaw-Fen Wang et al., 2013). Breeding for resistance QTL is
326 thus the primary way forward to developing *Ralstonia*-resistant crops in the Solanaceae. This has
327 not been easy, in part because of the diversity of *Ralstonia*. The *Ralstonia solanacearum* species
328 complex was recently subdivided into three species (*R. solanacearum*, *R. pseudosolanacearum*,
329 and *R. syzygii*), each prevalent in a different part of the world (Remenant et al., 2012; Safni et al.;
330 Prior et al., 2016). Each species has multiple strains, with an overlapping, but distinct set of
331 virulence proteins that promote disease (Landry et al., 2020). Varieties with effective resistance

332 will likely have QTL that are effective against local strains (strain-specific QTL) as well as those
333 effective against multiple strains (broad-spectrum QTL).
334
335 Most previously identified QTL have focused on resistance to *R. pseudosolanacearum*, and none
336 of them used the strain of *R. solanacearum* as in this work (Danesh et al., 1994; Thoquet et al.,
337 1996a, 1996b; Wang et al., 2000; Carmeille et al., 2006; Jaw-Fen Wang et al., 2013; Shin et al.,
338 2020; Mangin et al., 1999). Using visual assessment of wilting and the same RIL population of
339 tomato (H7996 x WV700) used here, one broad-spectrum QTL for resistance to multiple strains
340 of *R. pseudosolanacearum,* and one strain of *R. solanacearum* (JT-516) had been previously
341 identified on chromosome 6 (Danesh et al., 1994; Thoquet et al., 1996a, 1996b; Mangin et al.,
342 1999; Wang et al., 2000; Carmeille et al., 2006; Jaw-Fen Wang et al., 2013; Shin et al., 2020).
343 We also identified a QTL on chromosome 6, using visual assessment in both 2016 and 2019. In
344 our study, *Bwr6.1* confers 8 – 11% of the variation, compared to 11.5 – 33% for *Bwr6a - Bwr6d*
345 (Jaw-Fen Wang et al., 2013; Shin et al., 2020). The genes within the left and right intervals of
346 *Bwr6.1* are particularly interesting because there are two groups of NBS-LRRs located between
347 the left and right markers for *Bwr6.1* (solcap_snp_sl_14458 and the GBS-identified SNP at
348 39435402). One of these groups includes the *S. lycopersicum* homolog of Arabidopsis
349 *RESISTANCE to PSEUDOMONAS SYRINGAE 4* (*RPS4*). Fine-mapping of *Bwr6.1* is needed to
350 determine whether a specific NBS-LRR protein or receptor is responsible for the resistance
351 conferred by this region.
352
353 Previous studies also identified a major QTL on chromosome 12 that is effective for resistance to
354 *R. pseudosolanacearum*, and explained between 15.9 – 53.9% of the variation (Shin et al., 2020).
355 We found two clusters of QTL on chromosome 12, for image-based traits. Within the region
356 spanning *Bwr12.1* on chromosome 12 is one NBS-LRR disease resistance gene (*Solyc12g10740*)
357 and one receptor-like kinase (*Solyc12g010660*) while within *Bwr12.2* are genes related to disease
358 resistance pathways, including a gene encoding a Pathogenesis Response (PR) Protein
359 (*Solyc12g014310*), and two genes encoding Leucine Rich Repeat – Receptor Like Kinases
360 (*Solyc12g014350* and *Solyc12g150105*). Our results suggest that this region of chromosome 12
361 may be important for resistance to multiple strains of *Ralstonia*. The QTL we identified on
362 chromosomes 2, 3, 4, 5, 8 and 10 were not previously identified, and thus may be specific to *R.*

363 *solanacearum* strain K60. With the exception of *Bwr3.2*, these QTL were detected using only
364 our image-based traits.
365
366 Together, our results establish the value of image-based, non-destructive disease phenotyping for
367 uncovering novel genetic components and new targets for quantitative disease resistance in
368 crops. By identifying new genetic loci, this type of rapid phenotyping may enable the
369 identification of broad-spectrum and durable resistance.
370
371 **Methods**
372 ***Plant growth***
373 Seeds of 188 Hawaii7996 (H7996) x West Virginia700 (WV) recombinant inbred lines (RILs) in
374 the F8 generation were obtained from the Asian Vegetable Research and Development Center
375 (AVRDC) in June 2014. Seeds were propagated to the F_9 generation in field and greenhouse in
376 West Lafayette, IN in 2014 and 2015 and were used in QTL analysis in 2016 and 2019.
377
378 For all plants used in the imaging experiments and 2019 visual assessment of wilting, seeds were
379 sown into individually labeled 1801 traditional inserts that were placed into 1020 flats (Hummert
380 International, USA). Seeds in the 2016 experiment were sown into individually labeled 1203
381 inserts that were placed into 1020 flats. Seeds were sown into ProMix Propagation Mix supplied
382 by the Lilly Greenhouses and Growth Facility located at Purdue University, West Lafayette,
383 Indiana, USA. The individual pots were randomized and placed in a growth chamber at 28ºC,
384 relative humidity of 65% for a lighting cycle of 16 hours light/8 hours dark. The plants began
385 germination on day 4 and plants were inoculated with *R. solanacearum* strain K60 at 17 days
386 after planting when three true leaves were present. Trays were rotated in the growth chamber
387 throughout each experiment. In 2016, four seeds of each RIL were grown in the growth chamber
388 with parental controls, and each plant was visually assessed for wilting at 8 days post inoculation
389 (dpi). In 2019, one seed per RIL, along with parental controls, was grown in the growth chamber
390 for each of five independent replicates. Each plant was imaged at -1, 3, 4, 5, and 6 dpi, and
391 visually assessed at 8 dpi.
392

393 For plants used to genotyping with tomato SolCap markers, F_9 generation RIL seeds and parental
394 controls were grown in the greenhouse in 2-gallon pots with Metro Mix 510 soil. Plants were
395 grown for 6 weeks.
396
397 ***Ralstonia solanacearum growth and plant inoculation***
398 *Ralstonia solanacearum* strain K60 (containing a GFP reporter) was grown on casamino acid-
399 peptone-glucose (CPG) agar containing tetrazolium chloride (TZC) in the dark for 48 hours at
400 28ºC as in (Caldwell et al., 2017). Briefly, bacteria were resuspended in sterile water to a
401 concentration of approximately 2 x 10^8 colony forming units (CFU)/mL for each experiment. For
402 each experiment, the concentration of inoculum was confirmed through dilution plating. Pots of
403 three-leaf plants were lightly compressed to induce wounding similar to transplant handling in
404 field conditions. 60 mL of inoculum was applied to the surrounding soil using a serological
405 pipet.
406
407 ***Visual assessment of bacterial wilt disease***
408 Wilt scores were visually assessed 8 dpi. Wilt scores were calculated by counting the number of
409 wilted true leaves divided by the total number of true leaves on the plant. Plants were scored with
410 a 95% if the plant had all of its leaves wilted, excluding the topmost leaf. Plants were marked as
411 100% when the topmost portion of the stem was collapsed and wilted (Supplemental Figure 2).
412
413 ***Plant imaging***
414 Plants were imaged the day before inoculation (-1 dpi) and then imaged on 3, 4, 5, and 6 dpi. A
415 Linco Linstor 2000-watt photo studio (Amazon, USA) was used as the backdrop, and Flora X
416 fluorescent lighting (Amazon, USA) was used to create a small photo studio. Individual plants
417 were placed on a Photocapture 360 turntable (Ortery Technologies) that was programmed to
418 capture eight images around the plant (every 45°). The images were captured using an EOS 6D
419 Canon camera with an EF 50mm f/1.4 USM lens on a stationary tripod. An imaging carriage
420 was created with a square petri dish and a fiducial marker attached to each side. A total of five
421 independent replicates for each RIL and the parental controls were imaged.
422
423 ***Phenotyping Pipeline and Image Analysis***

From the plant images, ten traits were acquired for QTL analysis. A detailed description of the acquisition process can be found in (Yang et al., 2021, 2020). All traits were extracted based on plant color and shape. To eliminate any color discrepancy between images, images were automatically color corrected using a fiducial marker consisting of a colored checkerboard with known physical dimensions and colors.

After color correction, plant pixels were segmented from the rest of the image by thresholding channels in the L*A*B* color space. The resulting segmentation mask was improved with image morphological operations to fill holes and remove noise generated by the thresholding. The stem of the plant was identified using two neural networks, Mask R-CNN and U-Net. By locating the stem of the plant, metrics were defined that reflect the inner morphology of the plant. To train the neural networks, stem segmentation ground truth data were generated using Adobe Photoshop and LabelMe (a Python-based annotation tool) to mark the location of the image pixels belonging to the stem of the plant. Further details about this procedure are described in (Yang et al., 2020, 2021).

The plant and stem masks were used in the subsequent color and shape analysis, which acquired ten traits: total area of the plant mask (plant area), height of the plant mask (plant height), maximum width of the plant mask (plant width), area of the convex hull (convex area), width of the convex hull (convex width), color-based weighted average (color average), horizontal distance between the center of mass of the left and right sides of the plant stem (CM width), height of the center of mass (CM height), x-axis distribution of the center of mass (X mass), Y-axis distribution of the center of mass (Y mass).

The plant area, plant height and plant width were calculated from the plant mask. When calculating plant height, the upper 5% of the plant material was not included, which helped eliminate the impact of small leaves growing at the top. Using functions available in *OpenCV* Python Library, a convex hull was fit around the plant mask and the convex area and convex width were calculated. For color analysis, the weighted average of the pixel values in the A* channel was calculated, as this channel captures the green-magenta spectrum.

455 To calculate traits involving the center of mass (CM), the plant mask was split into left and right
456 halves using the stem mask (Yang et al., 2020), and the CM located for each half. The x-axis
457 distance between CMs (CM width) and the average height of the CMs (CM height) were used as
458 traits.
459
460 The extension of just one leaf can have a major impact on measured plant width, generating a
461 disproportionately larger value. Capturing the plant material distribution inside the plant mask
462 can overcome this issue. Using the split plant mask, the horizontal and vertical distribution of
463 plant material was estimated. The distances at which 90% of the plant material was captured in
464 the horizontal and vertical directions were used as the traits 'X mass distribution' and 'Y mass
465 distribution'. The average of eight views around the plant were used for each trait value. Outputs
466 are in pixels.
467
468 In the random forest classification, visual wilting scores were thresholded to 0 or 1, where 0 = 0
469 to 50% wilting, 1 = 51 – 100% wilting. Average trait values from eight views from 6 dpi for 969
470 plants (RILs and parental controls) were used across all five replicates. Some plants did not have
471 a trait value for that day and were not used in the algorithm.
472
473 ***DNA extraction, Marker generation and Genotyping by Sequencing (GBS)***
474 Tomato SolCap markers and single nucleotide polymorphisms (SNPs) identified through GBS
475 were used for map creation. Leaf disc samples were collected from each RIL plant using a
476 biopsy punch and were sent to LGC, Biosearch Technologies. Genomic DNA was extracted and
477 genotyped for 128 SNPs from the Tomato SolCAP panel using LGC's KASP assay. One
478 hundred twelve SNPs were obtained for RILs using this method.
479
480 For GBS, genomic DNA (gDNA) was extracted from 188 F_9 individuals of the RIL population
481 and from parental plants using Trizol. gDNA was RNase-treated and cleaned with phenol
482 chloroform extraction. Sequencing library preparation was as described by (Elshire et al., 2011).
483 Briefly, gDNA was digested with *PstI* and 150 bp paired end sequencing was performed on two
484 lanes of an Illumina Hi-seq 2500 at the Purdue Genomics Facility.
485

486 Reads were mapped to the *Solanum lycopersicum* 3.0 genome using the methods of (Manching
487 et al., 2017). In brief, reads were de-multiplexed, and adapter sequences were removed. Reads
488 were filtered based on the presence of a GBS barcode on the forward read (R1), which accounts
489 for 95.4% of the PE reads. For these R1, 97.3% had a paired R2 read, and 2.7% did not have a
490 pair. R1 read pairs and R1 singles reads were combined and assessed independent of pairing and
491 treated as single end reads for the remaining analyses (924,500,737 reads).
492
493 Reads were filtered to remove those with the presence of an internal restriction site, the lack of
494 restriction site hang sequence at the end, and for minimum length, which retained 93.0% of the
495 reads. There was a minimum of 17,561 reads, a maximum of 16,127,292 reads, and an average
496 of 4,480,149 reads per sample (Supplemental Figure 8). Reads were mapped using BWA-MEM
497 for paired end reads, and the GATK haplotype caller was used to generate a genomic Variant
498 Call Format (gVCF) file for downstream analysis.
499 There were 74,082 SNPs called between the population and *Solanum lycopersicum* 3.0 reference
500 genome. Many of these were SNPs between the reference genome and the population and do not
501 vary in the population used here. Filtering for the presence of two alleles within the RIL
502 population identified resulted in 2,738 SNPs. Of these, the parental alleles were identified in
503 both parents for 278 SNPs and in one parent for 698 SNPs. The remaining 1,762 SNPs could not
504 be assigned a parental origin and were not used for further analysis. The 976 SNPs with parental
505 origin identified were filtered for a minor allele frequency greater than 0.02 and less than 0.99,
506 which resulted in 632 high quality SNPs.
507
508 High quality SNPs identified from GBS were combined with previously defined SolCap markers
509 from LGC Biosearch Technologies for a total of 748 markers. SNP coverage of the 188 RIL taxa
510 was high. Of the 748 markers, the minimum coverage was 115 markers, the maximum coverage
511 was 555 markers, and the average was 366 markers (Supplemental Figure 9). There was some
512 residual heterozygosity in the taxa (Supplemental Figure 9b), and taxa with 10% or greater
513 heterozygosity were removed from further analysis (2 RILs).
514
515 ***Linkage Map Construction***

516 The software QTL IciMapping (Meng et al., 2015) (version 4.1) was used for the map
517 construction with all 748 markers. Redundant markers were filtered by taxa coverage using a
518 missing rate of 85% and a distortion threshold at 0.001 to obtain a total of 408 markers. The 408
519 markers without anchor information were assigned to 12 groups based on a LOD score threshold
520 value of 3. After grouping, the markers were ordered using the nearest neighbor algorithm
521 (nnTwoOpt) using the rippling criterion SARF (Sum of Adjacent Recombination Frequencies)
522 with a window size of five markers. After ordering, some markers at the end of the chromosomes
523 were deleted when they were adding an insignificant genetic distance to the chromosome. These
524 markers were identified after splitting the current chromosome in two sub-chromosomes between
525 the longest marker interval. If the shortest sub-chromosome contained more than 20% of the
526 markers before splitting, the two sub-chromosome were re-assembled. Otherwise, the shortest
527 sub-chromosome was deleted.
528
529 ***QTL detection***
530 QTL were detected using Inclusive Composite Interval Mapping with additive effects (ICIM-
531 ADD) in IciMapping (Meng et al., 2015) (version 4.1) using a genetic mapping with a 1 cM
532 scanning step and a probability in stepwise regression of 0.001. The LOD significance threshold
533 to declare a QTL significant was determined using a Type-I error of 0.0500 after one thousand
534 permutation. For the QTL analysis, we removed 19 of the 188 RIL (10%) showing the highest
535 variation according to the visual wilting score and 3 RIL due to missing data across the 5
536 biological repetitions for a total of 166 RIL into the QTL map (Supplemental Figure 3). The
537 evolution of the ten image-based traits and two visual wilting scores between -1 dpi and 3, 4, 5
538 and 6 dpi were determined for the 166 RIL. To assure a normal distribution of the phenotypic
539 data, the function "orderNorm" was used to perform an ordered quantile normalization (Peterson
540 and Cavanaugh, 2020) before QTL analysis using the package "bestNormalize" version 1.6.1
541 with R software version 3.6.1 (R Core Team).
542
543 **Acknowledgements**
544 We thank Chloe Caldwell for help with imaging, and Kristina Gans for help with GBS.

This work was funded by a Purdue Seed Grant to AIP and ED, a Foundation for Food and Agriculture Research New Innovator Award to AIP, and the endowment of the Charles William Harrison Distinguished Professorship at Purdue University to ED.

Author Contributions

A.I.P. and E.D. designed the research; V.M., D.C., and B.K. performed research; V.M, E.E., S.B., C.Y, A.I.P, and E.J.D. analyzed data; S.B., C.Y., and E.D. contributed new computational tools; A.I.P. and V.M. wrote the manuscript; all authors edited and approved the manuscript.

References

Awata, L.A.O., Beyene Y., Gowda M., Suresh L.M., Jumbo M.B. Tongoona P., Danquah E., Ifie B.E., Marchelo-Dragga P.W., Olsen M., Ogugu V. et al. (2020). Genetic Analysis of QTL for Resistance to Maize Lethal Necrosis in Multiple Mapping Populations. Genes 11: 32.

Awlia, M., Alshareef, N., Saber, N., Korte, A., Oakey, H., Panzarová, K., Trtílek, M., Negrão, S., Tester, M., and Julkowska, M.M. (2021).Genetic mapping of the early responses to salt stress in *Arabidopsis thaliana*. Plant J. doi:10.1111/tpj.15310.

Bock, C., Parker, P., Cook, A.Z., and Gottwald, T. (2008). Visual Rating and the Use of Image Analysis for Assessing Different Symptoms of Citrus Canker on Grapefruit Leaves. Plant Dis 92:530-541.

Bock, C., Poole, G., Parker, P., and Gottwald, T.R. (2010). Plant Disease Severity Estimated Visually, by Digital Photography and Image Analysis, and by Hyperspectral Imaging. Crit Rev Plant Sci 29: 59-107.

Caldwell, D., Kim, B.-S., and Iyer-Pascuzzi, A.S. (2017). *Ralstonia solanacearum* Differentially Colonizes Roots of Resistant and Susceptible Tomato Plants. Phytopathology 107: 528–536.

Carmeille, A., Caranta, C., Dintinger, J., Prior, P., Luisetti, J., and Besse, P. (2006). Identification of QTLs for *Ralstonia solanacearum* race 3-phylotype II resistance in tomato. Theor Appl Genet 113: 110–21.

Colwell, R.N. (1956). Determining the prevalence of certain cereal crop diseases by means of aerial photography. Hilgardia 26: 223–286.

Corwin, J.A., Copeland, D., Feusier, J., Subedy, A., Eshbaugh, R., Palmer, C., Maloof, J., and Kliebenstein, D.J. (2016). The Quantitative Basis of the Arabidopsis Innate Immune

System to Endemic Pathogens Depends on Pathogen Genetics. PLoS Genet 12: e1005789.

Danesh, D., Aarons, S., McGill, G.E., and Young, N.D. (1994). Genetic Dissection of Oligogenic Resistance to Bacterial Wilt in Tomato. Mol Plant Microbe Interact 7: 464–471.

Elshire, R.J., Glaubitz, J.C., Sun, Q., Poland, J.A., Kawamoto, K., Buckler, E.S., and Mitchell, S.E. (2011). A Robust, Simple Genotyping-by-Sequencing (GBS) Approach for High Diversity Species. PLOS ONE 6: e19379.

Fordyce, R.F., Soltis, N.E., Caseys, C., Gwinner, R., Corwin, J.A., Atwell, S., Copeland, D., Feusier, J., Subedy, A., Eshbaugh, R., and Kliebenstein, D.J. (2018). Digital Imaging Combined with Genome-Wide Association Mapping Links Loci to Plant-Pathogen Interaction Traits. Plant Physiol 178: 1406–1422.

Genin, S. (2010). Molecular traits controlling host range and adaptation to plants in *Ralstonia solanacearum*. New Phytol 187: 920–928.

Genin, S. and Denny, T.P. (2011). Pathogenomics of the *Ralstonia solanacearum* Species Complex. Annu Rev Phytopathol 50: 67–89.

Jackson, R.D. (1986). Remote Sensing of Biotic and Abiotic Plant Stress. Annu Rev Phytopathol 24: 265–287.

Jaw-Fen Wang, Fang-I Ho, Hai Thi Hong Truong, Shu-Mei Hugan, Conrado H. Balatero, Vanla Dittapongpitch, and Nurul Hidayati (2013). Identification of major QTLs associated with stable resitance of tomato cultivar “Hawaii 7996” to *Ralstonia solanacearum*. Euphytica 190: 241–252.

Knoch, D., Abbadi, A., Grandke, F., Meyer, R.C., Samans, B., Werner, C.R., Snowdon, R.J., and Altmann, T. (2020). Strong temporal dynamics of QTL action on plant growth progression revealed through high-throughput phenotyping in canola. Plant Biotechnol J 18: 68–82.

Landry, D., González-Fuente, M., Deslandes, L., and Peeters, N. (2020). The large, diverse, and robust arsenal of *Ralstonia solanacearum* type III effectors and their in planta functions. Mol. Plant Pathol. doi:10.1111/mpp.12977

Li, H., Feng, H., Guo, C., Yang, S., Huang, W., Xiong, X., Liu, J., Chen, G., Liu, Q., Xiong, L., Liu, K., and Yang, W. (2020). High-throughput phenotyping accelerates the dissection of the dynamic genetic architecture of plant growth and yield improvement in rapeseed. Plant Biotechnol J 18: 2345–2353.

Lowe, A., Harrison, N., and French, A.P. (2017). Hyperspectral image analysis techniques for the detection and classification of the early onset of plant disease and stress. Plant Methods 13: 80.

615 Mahlein, A.-K. (2016). Plant Disease Detection by Imaging Sensors - Parallels and Specific
616 Demands for Precision Agriculture and Plant Phenotyping. Plant Dis. 100: 241-251.

617 Mahlein, A.-K., Alisaac, E., Al Masri, A., Behmann, J., Dehne, H.-W., and Oerke, E.-C. (2019).
618 Comparison and Combination of Thermal, Fluorescence, and Hyperspectral Imaging for
619 Monitoring Fusarium Head Blight of Wheat on Spikelet Scale. Sensors 19: 2281.

620 Mahlein, A.-K., Kuska, M., Thomas, S., Bohnenkamp, D., Alisaac, E., Behmann, J., Wahabzada,
621 M., and Kersting, K. (2017). Plant disease detection by hyperspectral imaging: from the
622 lab to the field. Adv Anim Biosci 8: 238-243.

623 Manching, H., Sengupta, S., Hopper, K.R., Polson, S.W., Ji, Y., and Wisser, R.J. (2017). Phased
624 Genotyping-by-Sequencing Enhances Analysis of Genetic Diversity and Reveals
625 Divergent Copy Number Variants in Maize. G3 Genes Genom Genet 7: 2161–2170.

626 Mangin, B., Thoquet, P., Olivier, J., and Grimsley, N.H. (1999). Temporal and multiple
627 quantitative trait loci analyses of resistance to bacterial wilt in tomato permit the
628 resolution of linked loci. Genetics 151: 1165–1172.

629 Mansfield, J. et al. (2012). Top 10 plant pathogenic bacteria in molecular plant pathology. Mol
630 Plant Pathol 13: 614–629.

631 Maschietto, V., Colombi, C., Pirona, R., Pea, G., Strozzi, F., Marocco, A., Rossini, L., and
632 Lanubile, A. (2017). QTL mapping and candidate genes for resistance to Fusarium ear rot
633 and fumonisin contamination in maize. BMC Plant Biology 17: 20.

634 Meng, L., Li, H., Zhang, L., and Wang, J. (2015). QTL IciMapping: Integrated software for
635 genetic linkage map construction and quantitative trait locus mapping in biparental
636 populations. Crop J 3: 269–283.

637 Mir, R.R., Reynolds, M., Pinto, F., Khan, M.A., and Bhat, M.A. (2019). High-throughput
638 phenotyping for crop improvement in the genomics era. Plant Sci 282: 60–72.

639 Mochida, K., Koda, S., Inoue, K., Hirayama, T., Tanaka, S., Nishii, R., and Melgani, F. (2019).
640 Computer vision-based phenotyping for improvement of plant productivity: a machine
641 learning perspective. GigaScience 8.

642 Pauli, D., Andrade-Sanchez, P., Carmo-Silva, A.E., Gazave, E., French, A.N., Heun, J.,
643 Hunsaker, D.J., Lipka A.E., Setter, T.L., Strand, R.J. et al. (2016). Field-Based High-
644 Throughput Plant Phenotyping Reveals the Temporal Patterns of Quantitative Trait Loci
645 Associated with Stress-Responsive Traits in Cotton. G3 Genes Genom Genet 6: 865–879.

646 Pérez-Bueno, M.L., Pineda, M., and Barón, M. (2019). Phenotyping Plant Responses to Biotic
647 Stress by Chlorophyll Fluorescence Imaging. Front. Plant Sci. 10.

648 Peterson, R.A. and Cavanaugh, J.E. (2020). Ordered quantile normalization: a semiparametric
649 transformation built for the cross-validation era. J Applied Stat 47: 2312–2327.

650 Pineda, M., Barón, M., and Pérez-Bueno, M.-L. (2021). Thermal Imaging for Plant Stress
651 Detection and Phenotyping. Remote Sens 13: 68.

652 Prior, P., Ailloud, F., Dalsing, B.L., Remenant, B., Sanchez, B., and Allen, C. (2016). Genomic
653 and proteomic evidence supporting the division of the plant pathogen *Ralstonia*
654 *solanacearum* into three species. BMC Genomics 17: 90.

655 R Core Team R: A language and environment for statistical computing. R Foundation for
656 Statistical Computing Vienna: URL https://www.R-project.org/.

657 Remenant, B., Babujee, L., Lajus, A., Médigue, C., Prior, P., and Allen, C. (2012). Sequencing
658 of K60, Type Strain of the Major Plant Pathogen *Ralstonia solanacearum*. J Bacteriol
659 194: 2742–2743.

660 Safni, I., Cleenwerck, I., De Vos, P., Fegan, M., Sly, L., and Kappler, U. 2014 Polyphasic
661 taxonomic revision of the *Ralstonia solanacearum* species complex: proposal to emend
662 the descriptions of *Ralstonia solanacearum* and *Ralstonia syzygii* and reclassify current
663 *R. syzygii* strains as *Ralstonia syzygii* subsp. syzygii subsp. nov., *R. solanacearum*
664 phylotype IV strains as *Ralstonia syzygii* subsp. indonesiensis subsp. nov., banana blood
665 disease bacterium strains as *Ralstonia syzygii* subsp. celebesensis subsp. nov. and *R.*
666 *solanacearum* phylotype I and III strains as *Ralstonia pseudosolanacearum* sp. nov. Int J
667 Syst Evol Microbiol 64: 3087–3103.

668 Schandry, N. (2017). A Practical Guide to Visualization and Statistical Analysis of R.
669 solanacearum Infection Data Using R. Front. Plant Sci. 8.

670 Shakoor, N., Lee, S., and Mockler, T.C. (2017). High throughput phenotyping to accelerate crop
671 breeding and monitoring of diseases in the field. Curr Opin Plant Biol 38: 184–192.

672 Shin, I.S., Hsu, J.-C., Huang, S.-M., Chen, J.-R., Wang, J.-F., Hanson, P., and Schafleitner, R.
673 (2020). Construction of a single nucleotide polymorphism marker based QTL map and
674 validation of resistance loci to bacterial wilt caused by *Ralstonia solanacearum* species
675 complex in tomato. Euphytica 216: 54.

676 Simko, I., Jimenez-Berni, J.A., and Sirault, X.R.R. (2017). Phenomic Approaches and Tools for
677 Phytopathologists. Phytopathology 107: 6–17.

678 Stewart, E. and McDonald, B. (2014). Measuring quantitative virulence in the wheat pathogen
679 *Zymoseptoria tritici* using high-throughput automated image analysis. Phytopathology
680 104: 985-992.

681 Stewart, E.L., Hagerty, C.H., Mikaberidze, A., Mundt, C.C., Zhong, Z., and McDonald, B.A.
682 (2016). An Improved Method for Measuring Quantitative Resistance to the Wheat
683 Pathogen *Zymoseptoria tritici* Using High-Throughput Automated Image Analysis.
684 Phytopathology 106: 782–788.

685 Tanger, P., Klassen S., Mojica J.P., Lovell, J.T., Moyers, B.T., Baraoidan, M., Naredo, M.E.B.,
686 McNally, K.L., Poland, J., Bush, D.R. et al. (2017). Field-based high throughput

687 phenotyping rapidly identifies genomic regions controlling yield components in rice. Sci
688 Rep 7: 42839.

689 Thoquet, P., Olivier, J., Sperisen, C., Rogowsky, P., Laterrot, H., and Grimsley, N. (1996a).
690 Quantitative trait loci determining resistance to bacterial wilt in tomato cultivar
691 Hawaii7996. Mol Plant Microbe Interact 9: 826–836.

692 Thoquet, P., Olivier, J., Sperisen, C., Rogowsky, P., Prior, P., Anais, G., Mangin, B., Bazin, B.,
693 Nazer, R., and Grimsley, N. (1996b). Polygenic resistance of tomato plants to bacterial
694 wilt in the French West Indies. Mol Plant-Microbe Interact 9: 837–842.

695 Topp, C.N., Iyer-Pascuzzi, A.S., Anderson, J.T., Lee, C-R., Zurek, P.R., Symonova, O., Zheng
696 Y., Bucksch, A., Mileyko, Y., Galkovskyi, T., et al(2013). 3D phenotyping and
697 quantitative trait locus mapping identify core regions of the rice genome controlling root
698 architecture. Proc. Natl. Acad. Sci. U.S.A. 110: E1695-1704.

699 Wang, J.F., Olivier, J., Thoquet, P., Mangin, B., Sauviac, L., and Grimsley, N.H. (2000).
700 Resistance of tomato line Hawaii7996 to *Ralstonia solanacearum* Pss4 in Taiwan is
701 controlled mainly by a major strain-specific locus. Mol Plant-Microbe Interact 13: 6–13.

702 Wang, X. et al. (2019). Dynamic plant height QTL revealed in maize through remote sensing
703 phenotyping using a high-throughput unmanned aerial vehicle (UAV). Sci Rep 9: 3458.

704 Yang, C., Baireddy, S., Cai, E., Meline, V., Caldwell, D., Iyer-Pascuzzi, A.S., and Delp, E.J.
705 (2021). Image-Based Plant Wilting Estimation. arXiv:2105.12926 [cs].

706 Yang, C., Baireddy, S., Chen, Y., Cai, E., Caldwell, D., Méline, V., Iyer-Pascuzzi, A.S., and
707 Delp, E.J. (2020). Plant Stem Segmentation Using Fast Ground Truth Generation. In
708 2020 IEEE Southwest Symposium on Image Analysis and Interpretation (SSIAI), pp. 62–
709 65.

710 Yates, S., Mikaberidze, A., Krattinger, S.G., Abrouk, M., Hund, A., Yu, K., Studer, B., Fouche,
711 S., Meile, L., Pereira, D., Karisto, P., and McDonald, B.A. (2019). Precision Phenotyping
712 Reveals Novel Loci for Quantitative Resistance to Septoria Tritici Blotch. Plant
713 Phenomics 2019: 1–11.

714 Young, N.D. and Danesh, D. (1994). Understanding Bacterial Wilt Resistance in Tomato
715 through the Use of DNA Genetic-Markers. Bacterial Wilt: 145–155.

716 Zhang, N., Yang, G., Pan, Y., Yang, X., Chen, L., and Zhao, C. (2020). A Review of Advanced
717 Technologies and Development for Hyperspectral-Based Plant Disease Detection in the
718 Past Three Decades. Remote Sensing 12: 3188.

719 Zhang, X. et al. (2017). High-Throughput Phenotyping and QTL Mapping Reveals the Genetic
720 Architecture of Maize Plant Growth. Plant Physiol 173: 1554–1564.

721

722

Supplemental Information

Supplemental Figures

Supplemental Figure 1: Design of our low cost phenotyping platform including automatic turntable, backdrop, lightning and RGB camera.

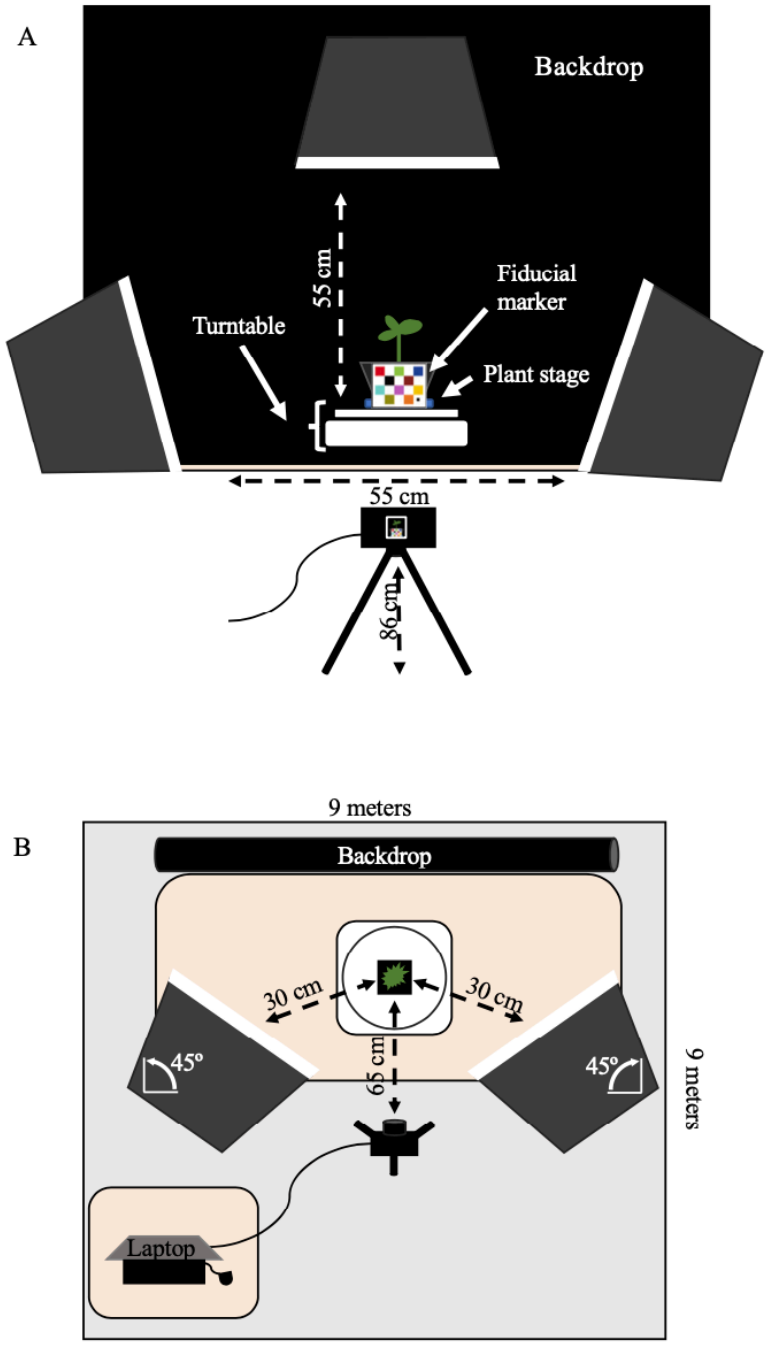

Supplemental Figure 2: Raw RGB pictures showing the evolution of wilting symptoms on RIL # 646 at -1, 3, 4, 5 and 6 dpi. Visually assessed wilting score are expressed in percentage of wilted leaves.

Supplemental Figure 3: Wilting Score RIL: Boxplots showing the normalized wilting score at 6 dpi for the 166 RILs, resistant Hawaii 7996 (HA) and susceptible West Virginia (WV) genotypes.

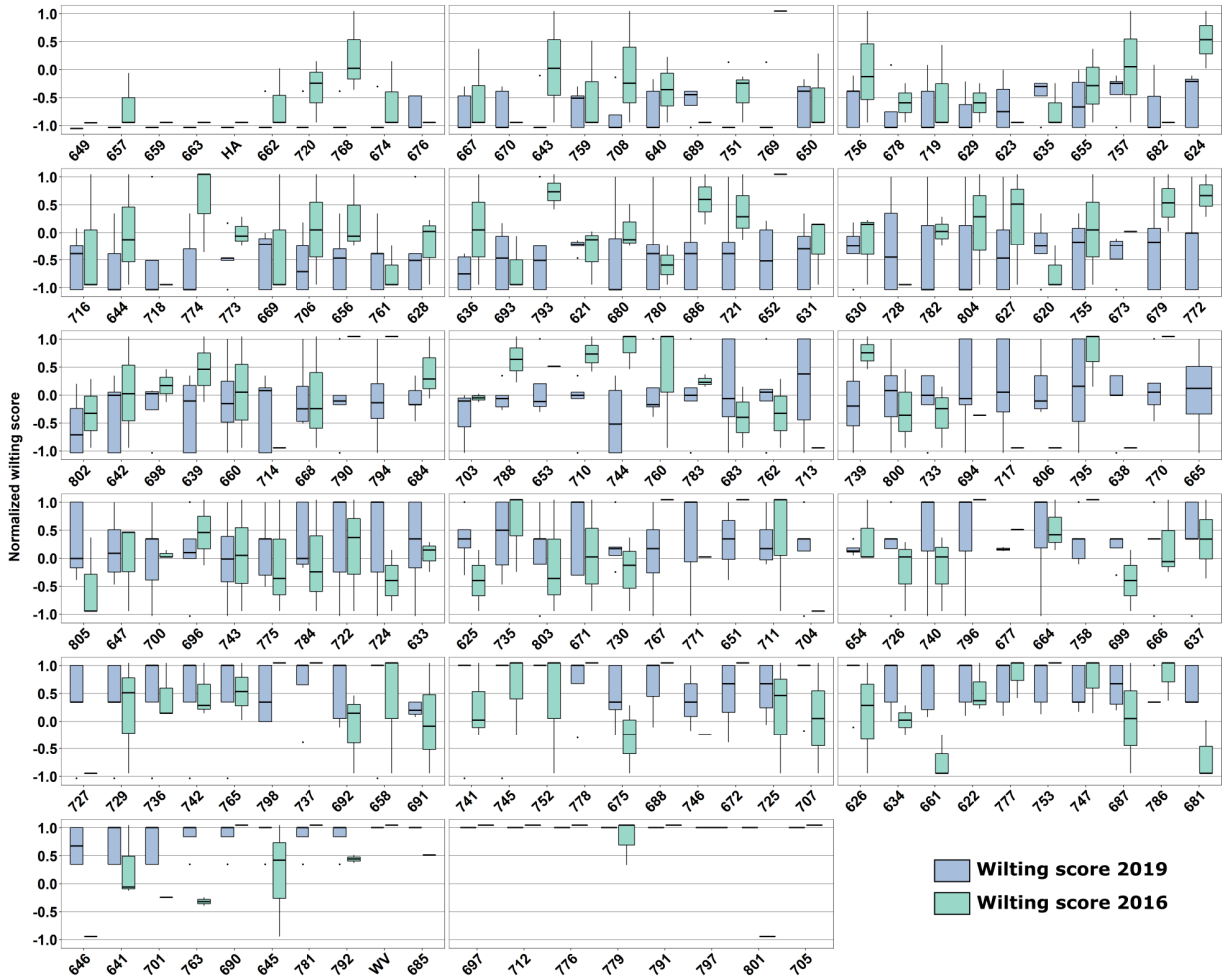

Supplemental Figure 4: RGB pictures showing the evolution of the traits at -1, 3, 4, 5 and 6 dpi for A) Hawaii 7996 and B) West Virginia (pw: plant width, ph: plant height, CMh: Center of Mass height, CMw: Center of Mass width, xm: Horizontal mass distribution, ym: Vertical mass distribution). The Hawaii 7996 plant shown here is the same plant used for Figure 1.

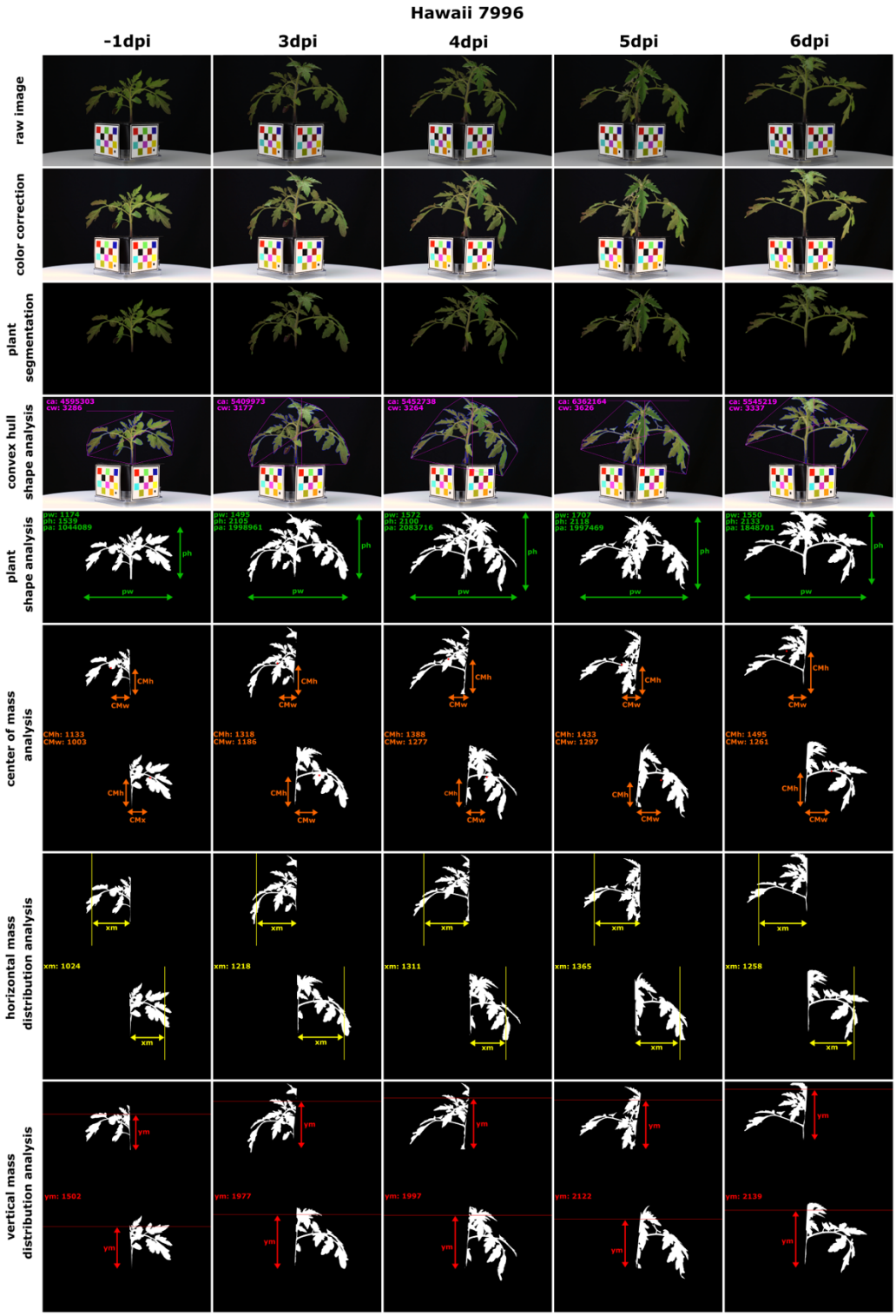
Hawaii 7996
-1dpi
3dpi
4dpi
5dpi
6dpi
raw image
color correction
plant segmentation
convex hull shape analysis
ca: 4595303
cw: 3286
ca: 5409973
cw: 3177
ca: 5452738
cw: 3264
ca: 6362164
cw: 3626
ca: 5545219
cw: 3337
plant shape analysis
pw: 1174
ph: 1539
pa: 1044089
pw: 1495
ph: 2105
pa: 1998961
pw: 1572
ph: 2100
pa: 2083716
pw: 1707
ph: 2118
pa: 1997469
pw: 1550
ph: 2133
pa: 1848701
ph
pw
center of mass analysis
CMh
CMw
CMx
CMh: 1133
CMw: 1003
CMh: 1318
CMw: 1186
CMh: 1388
CMw: 1277
CMh: 1433
CMw: 1297
CMh: 1495
CMw: 1261
horizontal mass distribution analysis
xm
xm: 1024
xm: 1218
xm: 1311
xm: 1365
xm: 1258
vertical mass distribution analysis
ym
ym: 1502
ym: 1977
ym: 1997
ym: 2122
ym: 2139

772

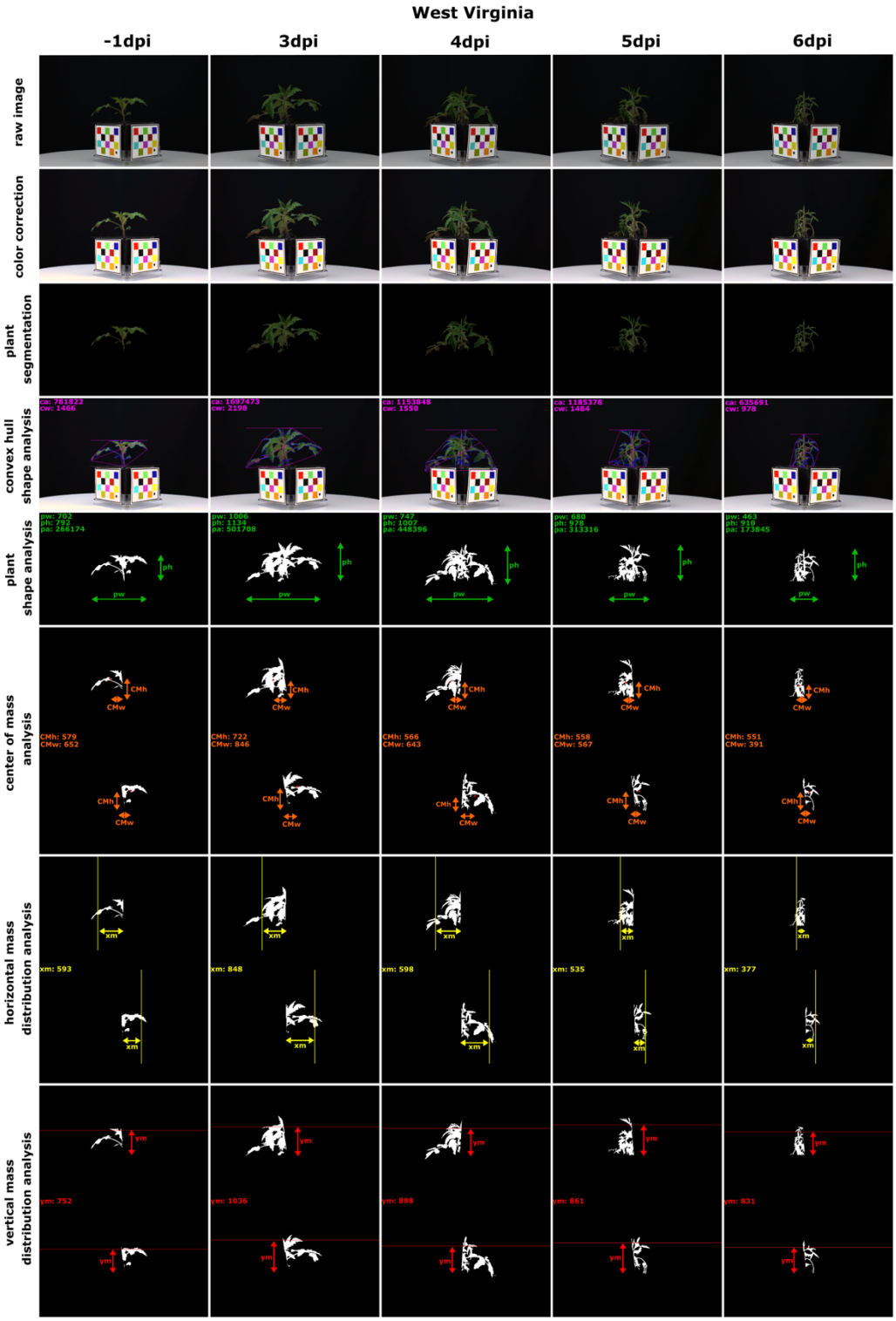
West Virginia
-1dpi
3dpi
4dpi
5dpi
6dpi
raw image
color correction
plant segmentation
convex hull shape analysis
ca: 781822
cw: 1466
ca: 1697473
cw: 2198
ca: 1153848
cw: 1550
ca: 1185378
cw: 1484
ca: 635691
cw: 978
plant shape analysis
pw: 702
ph: 797
pa: 266174
pw: 1006
ph: 1134
pa: 501708
pw: 747
ph: 1007
pa: 448396
pw: 680
ph: 978
pa: 313316
pw: 463
ph: 910
pa: 173845
center of mass analysis
CMh: 579
CMw: 652
CMh: 722
CMw: 846
CMh: 566
CMw: 643
CMh: 558
CMw: 567
CMh: 551
CMw: 391
horizontal mass distribution analysis
xm: 593
xm: 848
xm: 598
xm: 535
xm: 377
vertical mass distribution analysis
ym: 752
ym: 1036
ym: 898
ym: 861
ym: 831

Supplemental Figure 5: Boxplots showing the normalized values for image-based traits at -1, 3, 4, 5, 6 dpi for resistant Hawaii 7996, susceptible West Virginia 700, and 166 individuals of the RIL population.

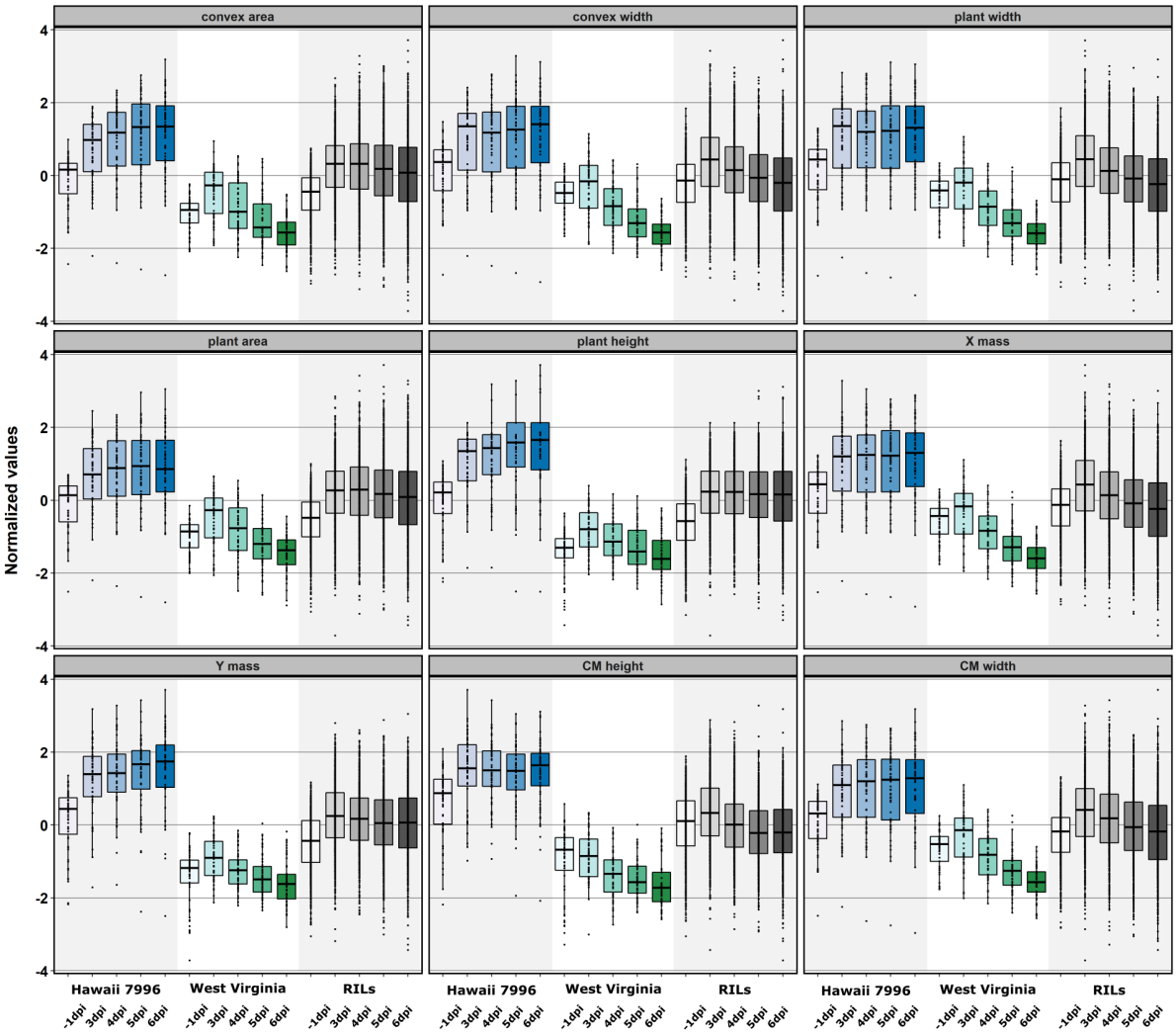

Supplemental Figure 6: Histogram showing the image-based descriptors which contribute the most to wilting

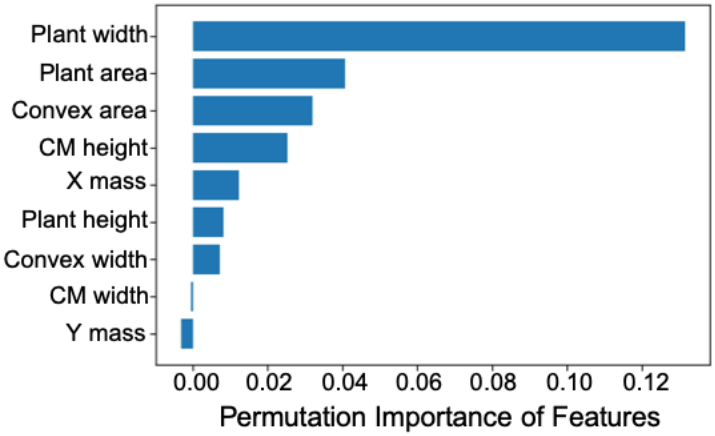

808 Supplemental Figure 7: Genetic Linkage map constructed with SolCap and SNP markers.
809 Location of 10 QTL clusters are displayed using blue and green for left and right markers
810 respectively. Location of previously identified QTL on chromosome 6 and 12[27] are also
811 displayed.
812
813
814
815
816

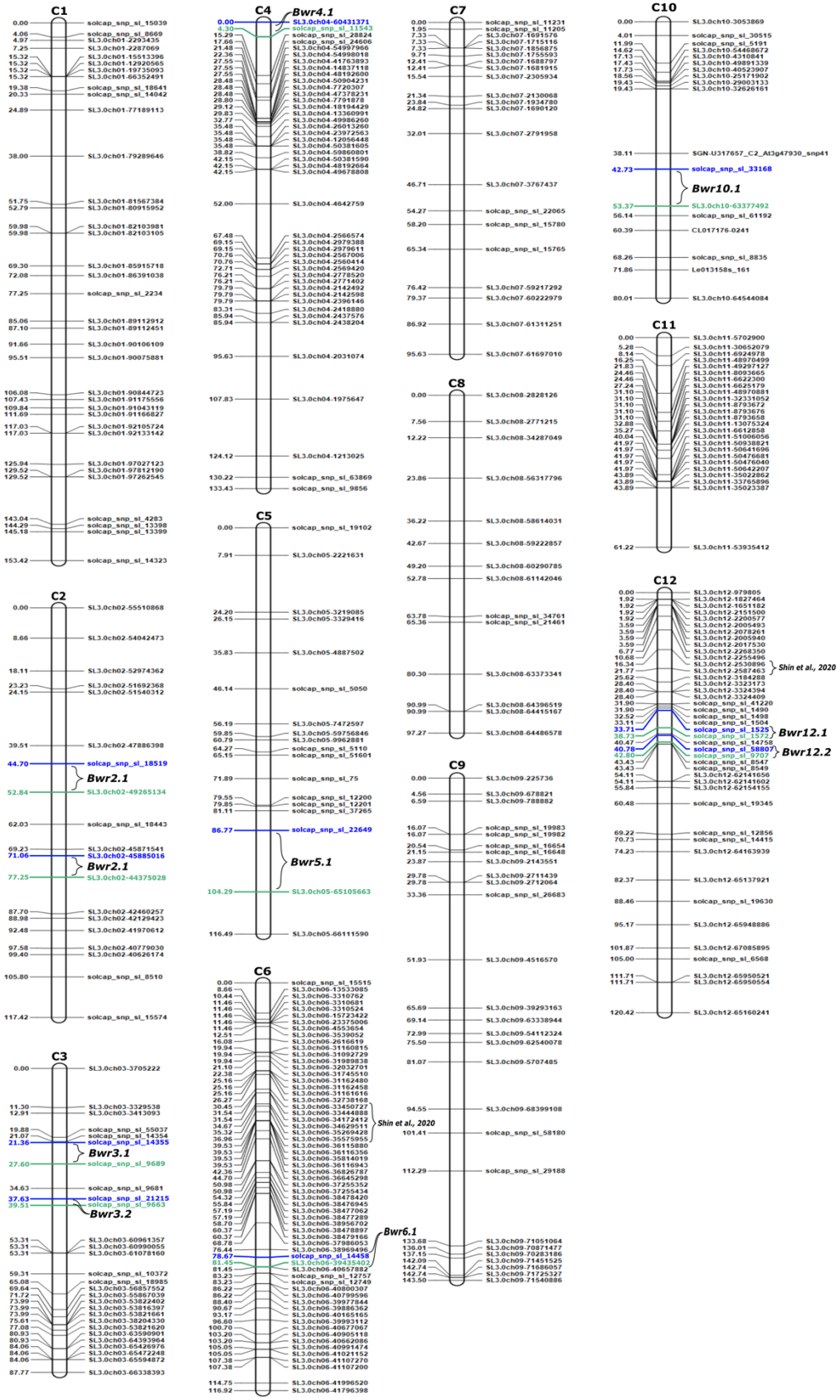
C1
0.00 solcap_snp_sl_15039
4.06 solcap_snp_sl_8669
4.97 SL3.0ch01-2293435
7.25 SL3.0ch01-2287069
15.32 SL3.0ch01-15513396
15.32 SL3.0ch01-12920565
15.32 SL3.0ch01-19735093
15.32 SL3.0ch01-66352491
19.38 solcap_snp_sl_18641
20.33 solcap_snp_sl_14042
24.89 SL3.0ch01-77189113
38.00 SL3.0ch01-79289646
51.75 SL3.0ch01-81567384
52.79 SL3.0ch01-80915952
59.98 SL3.0ch01-82103981
59.98 SL3.0ch01-82103105
69.30 SL3.0ch01-85915718
72.08 SL3.0ch01-86391038
77.25 solcap_snp_sl_2234
85.06 SL3.0ch01-89112912
87.10 SL3.0ch01-89112451
91.66 SL3.0ch01-90106109
95.51 SL3.0ch01-90075881
106.08 SL3.0ch01-90844723
107.43 SL3.0ch01-91175556
109.84 SL3.0ch01-91043119
111.69 SL3.0ch01-91166827
117.03 SL3.0ch01-92105724
117.03 SL3.0ch01-92133142
125.94 SL3.0ch01-97027123
129.52 SL3.0ch01-97812190
129.52 SL3.0ch01-97262545
143.04 solcap_snp_sl_4283
144.29 solcap_snp_sl_13398
145.18 solcap_snp_sl_13399
153.42 solcap_snp_sl_14323
C2
0.00 SL3.0ch02-55510868
8.66 SL3.0ch02-54042473
18.11 SL3.0ch02-52974362
23.23 SL3.0ch02-51692368
24.15 SL3.0ch02-51540312
39.51 SL3.0ch02-47886398
44.70 solcap_snp_sl_18519
Bwr2.1
52.84 SL3.0ch02-49265134
62.03 solcap_snp_sl_18443
69.23 SL3.0ch02-45871541
71.06 SL3.0ch02-45885016
Bwr2.1
77.25 SL3.0ch02-44375028
87.70 SL3.0ch02-42460257
88.98 SL3.0ch02-42129423
92.48 SL3.0ch02-41970612
97.58 SL3.0ch02-40779030
99.40 SL3.0ch02-40626174
105.80 solcap_snp_sl_8510
117.42 solcap_snp_sl_15574
C3
0.00 SL3.0ch03-3705222
11.30 SL3.0ch03-3329538
12.91 SL3.0ch03-3413093
19.88 solcap_snp_sl_55037
21.07 solcap_snp_sl_14354
21.36 solcap_snp_sl_14355
Bwr3.1
27.60 solcap_snp_sl_9689
34.63 solcap_snp_sl_9681
37.63 solcap_snp_sl_21215
39.51 solcap_snp_sl_9663
Bwr3.2
53.31 SL3.0ch03-60961357
53.31 SL3.0ch03-60990055
53.31 SL3.0ch03-61078160
59.31 solcap_snp_sl_10372
65.08 solcap_snp_sl_18985
69.64 SL3.0ch03-56857552
71.72 SL3.0ch03-55867039
73.99 SL3.0ch03-53822402
73.99 SL3.0ch03-53816397
73.99 SL3.0ch03-53821661
75.61 SL3.0ch03-38204330
77.08 SL3.0ch03-53821620
80.93 SL3.0ch03-63590901
80.93 SL3.0ch03-64393964
84.06 SL3.0ch03-65426976
84.06 SL3.0ch03-65472248
84.06 SL3.0ch03-65594872
87.77 SL3.0ch03-66338393
C4
Bwr4.1
0.00 SL3.0ch04-60431371
4.30 solcap_snp_sl_11543
15.29 solcap_snp_sl_28824
17.66 solcap_snp_sl_24606
21.48 SL3.0ch04-54997966
22.36 SL3.0ch04-54998018
27.55 SL3.0ch04-41763893
27.55 SL3.0ch04-14837118
27.55 SL3.0ch04-48192600
28.48 SL3.0ch04-50904231
28.48 SL3.0ch04-7720307
28.48 SL3.0ch04-47378231
28.80 SL3.0ch04-7791878
29.12 SL3.0ch04-18194429
29.83 SL3.0ch04-13360991
32.77 SL3.0ch04-49986260
35.48 SL3.0ch04-26013260
35.48 SL3.0ch04-23972563
35.48 SL3.0ch04-12056448
35.48 SL3.0ch04-50381605
38.82 SL3.0ch04-59860801
42.15 SL3.0ch04-50381590
42.15 SL3.0ch04-48192664
42.15 SL3.0ch04-49678808
52.00 SL3.0ch04-4642759
67.48 SL3.0ch04-2566574
69.15 SL3.0ch04-2979388
69.15 SL3.0ch04-2979611
70.76 SL3.0ch04-2567006
70.76 SL3.0ch04-2560414
72.71 SL3.0ch04-2569420
76.21 SL3.0ch04-2778520
76.21 SL3.0ch04-2771402
79.79 SL3.0ch04-2142492
79.79 SL3.0ch04-2142598
79.79 SL3.0ch04-2396146
83.31 SL3.0ch04-2418880
85.94 SL3.0ch04-2437576
85.94 SL3.0ch04-2438204
95.63 SL3.0ch04-2031074
107.83 SL3.0ch04-1975647
124.12 SL3.0ch04-1213025
130.22 solcap_snp_sl_63869
133.43 solcap_snp_sl_9856
C5
0.00 solcap_snp_sl_19102
7.91 SL3.0ch05-2221631
24.20 SL3.0ch05-3219085
26.15 SL3.0ch05-3329416
35.83 SL3.0ch05-4887502
46.14 solcap_snp_sl_5050
56.19 SL3.0ch05-7472597
59.85 SL3.0ch05-59756846
60.79 SL3.0ch05-9962881
64.27 solcap_snp_sl_5110
65.15 solcap_snp_sl_51601
71.89 solcap_snp_sl_75
79.55 solcap_snp_sl_12200
79.85 solcap_snp_sl_12201
81.11 solcap_snp_sl_37265
86.77 solcap_snp_sl_22649
Bwr5.1
104.29 SL3.0ch05-65105663
116.49 SL3.0ch05-66111590
C6
0.00 solcap_snp_sl_15515
8.66 SL3.0ch06-13533085
10.44 SL3.0ch06-3310762
11.46 SL3.0ch06-3310681
11.46 SL3.0ch06-3310524
11.46 SL3.0ch06-15723422
11.46 SL3.0ch06-23375006
11.46 SL3.0ch06-4553654
12.51 SL3.0ch06-3539052
16.08 SL3.0ch06-2616619
19.94 SL3.0ch06-31160815
19.94 SL3.0ch06-31092729
19.94 SL3.0ch06-31989838
21.10 SL3.0ch06-32032701
22.38 SL3.0ch06-31745510
25.16 SL3.0ch06-31162480
25.16 SL3.0ch06-31162458
25.16 SL3.0ch06-31161616
26.27 SL3.0ch06-32738168
30.45 SL3.0ch06-33450727
31.54 SL3.0ch06-33444888
31.54 SL3.0ch06-34172412
34.67 SL3.0ch06-34629511
35.32 SL3.0ch06-35269428
36.96 SL3.0ch06-35575955
39.53 SL3.0ch06-36115880
39.53 SL3.0ch06-36116356
39.53 SL3.0ch06-35814019
39.53 SL3.0ch06-36116943
42.36 SL3.0ch06-36826787
44.70 SL3.0ch06-36645298
50.98 SL3.0ch06-37255352
50.98 SL3.0ch06-37255434
54.32 SL3.0ch06-38478420
55.84 SL3.0ch06-38476945
57.19 SL3.0ch06-38477062
57.19 SL3.0ch06-38477289
58.70 SL3.0ch06-38956792
60.37 SL3.0ch06-38478887
60.37 SL3.0ch06-38479166
68.78 SL3.0ch06-37986053
76.44 SL3.0ch06-38969496
78.67 solcap_snp_sl_14458
81.45 SL3.0ch06-39435402
81.45 SL3.0ch06-40657882
83.23 solcap_snp_sl_12757
83.23 solcap_snp_sl_12749
86.22 SL3.0ch06-40800307
86.22 SL3.0ch06-40799596
88.40 SL3.0ch06-39977844
90.67 SL3.0ch06-39886362
93.17 SL3.0ch06-40165165
96.60 SL3.0ch06-39993112
100.70 SL3.0ch06-40677067
103.20 SL3.0ch06-40905118
103.20 SL3.0ch06-40662086
105.05 SL3.0ch06-40991474
105.05 SL3.0ch06-41021152
107.38 SL3.0ch06-41107270
107.38 SL3.0ch06-41107200
114.75 SL3.0ch06-41996520
116.92 SL3.0ch06-41796398
Shin et al., 2020
C7
0.00 solcap_snp_sl_11231
1.95 solcap_snp_sl_11205
7.33 SL3.0ch07-1691576
7.33 SL3.0ch07-1715116
7.33 SL3.0ch07-1856875
9.71 SL3.0ch07-1755593
12.41 SL3.0ch07-1688797
12.41 SL3.0ch07-1681915
15.54 SL3.0ch07-2305934
21.34 SL3.0ch07-2130068
23.84 SL3.0ch07-1934780
24.82 SL3.0ch07-1690120
32.01 SL3.0ch07-2791958
46.71 SL3.0ch07-3767437
54.27 solcap_snp_sl_22065
58.20 solcap_snp_sl_15780
65.34 solcap_snp_sl_15765
76.42 SL3.0ch07-59217292
79.37 SL3.0ch07-60222979
86.92 SL3.0ch07-61311251
95.63 SL3.0ch07-61697010
C8
0.00 SL3.0ch08-2828126
7.56 SL3.0ch08-2771215
12.22 SL3.0ch08-34287049
23.86 SL3.0ch08-56317796
36.22 SL3.0ch08-58614031
42.67 SL3.0ch08-59222857
49.20 SL3.0ch08-60290785
52.78 SL3.0ch08-61142046
63.78 solcap_snp_sl_34761
65.36 solcap_snp_sl_21461
80.30 SL3.0ch08-63373341
90.99 SL3.0ch08-64396519
90.99 SL3.0ch08-64415167
97.27 SL3.0ch08-64486578
C9
0.00 SL3.0ch09-225736
4.56 SL3.0ch09-678821
6.59 SL3.0ch09-788882
16.07 solcap_snp_sl_19983
16.07 solcap_snp_sl_19982
20.54 solcap_snp_sl_16654
21.15 solcap_snp_sl_16648
23.87 SL3.0ch09-2143551
29.78 SL3.0ch09-2711439
29.78 SL3.0ch09-2712064
33.36 solcap_snp_sl_26683
51.93 SL3.0ch09-4516570
65.69 SL3.0ch09-39293163
69.14 SL3.0ch09-63338944
72.99 SL3.0ch09-54112324
75.50 SL3.0ch09-62540078
81.07 SL3.0ch09-5707485
94.55 SL3.0ch09-68399108
101.41 solcap_snp_sl_58180
112.29 solcap_snp_sl_29188
Bwr6.1
133.68 SL3.0ch09-71051064
136.01 SL3.0ch09-70871477
137.15 SL3.0ch09-70283186
142.09 SL3.0ch09-71451525
142.74 SL3.0ch09-71686057
142.74 SL3.0ch09-71725327
143.50 SL3.0ch09-71540886
C10
0.00 SL3.0ch10-3053869
4.01 solcap_snp_sl_30515
11.99 solcap_snp_sl_5191
14.62 SL3.0ch10-54468672
17.13 SL3.0ch10-4310841
17.43 SL3.0ch10-49891339
17.73 SL3.0ch10-40523907
18.56 SL3.0ch10-25171902
19.43 SL3.0ch10-29003133
19.43 SL3.0ch10-32626161
38.11 SGN-U317657_C2_At3g47930_snp41
42.73 solcap_snp_sl_33168
Bwr10.1
53.37 SL3.0ch10-63377492
56.14 solcap_snp_sl_61192
60.39 CL017176-0241
68.26 solcap_snp_sl_8835
71.86 Le013158s_161
80.01 SL3.0ch10-64544084
C11
0.00 SL3.0ch11-5702900
5.28 SL3.0ch11-30652079
8.14 SL3.0ch11-6924978
16.25 SL3.0ch11-48970499
21.83 SL3.0ch11-49297127
24.46 SL3.0ch11-8093665
24.46 SL3.0ch11-6622300
27.24 SL3.0ch11-6625179
31.10 SL3.0ch11-48970881
31.10 SL3.0ch11-32331052
31.10 SL3.0ch11-8793672
31.10 SL3.0ch11-8793676
31.10 SL3.0ch11-8793658
32.88 SL3.0ch11-13075324
35.27 SL3.0ch11-6612858
40.04 SL3.0ch11-51006056
41.97 SL3.0ch11-50938821
41.97 SL3.0ch11-50641696
41.97 SL3.0ch11-50476681
41.97 SL3.0ch11-50476040
41.97 SL3.0ch11-50642207
43.89 SL3.0ch11-35022862
43.89 SL3.0ch11-33765896
43.89 SL3.0ch11-35023387
61.22 SL3.0ch11-53935412
C12
0.00 SL3.0ch12-979805
1.92 SL3.0ch12-1827464
1.92 SL3.0ch12-1651182
1.92 SL3.0ch12-2151500
1.92 SL3.0ch12-2200577
3.59 SL3.0ch12-2005493
3.59 SL3.0ch12-2078261
3.59 SL3.0ch12-2005940
3.59 SL3.0ch12-2017530
6.77 SL3.0ch12-2268350
10.68 SL3.0ch12-2255496
16.34 SL3.0ch12-2530896
21.77 SL3.0ch12-2587463
25.62 SL3.0ch12-3184288
28.40 SL3.0ch12-3323173
28.40 SL3.0ch12-3324394
28.40 SL3.0ch12-3324409
31.90 solcap_snp_sl_41220
31.90 solcap_snp_sl_1490
32.52 solcap_snp_sl_1498
33.11 solcap_snp_sl_1504
33.71 solcap_snp_sl_1525
38.73 solcap_snp_sl_1572
40.47 solcap_snp_sl_14758
40.78 solcap_snp_sl_58807
42.80 solcap_snp_sl_9707
43.43 solcap_snp_sl_8547
43.43 solcap_snp_sl_8549
54.11 SL3.0ch12-62141656
54.11 SL3.0ch12-62141602
55.84 SL3.0ch12-62154155
60.48 solcap_snp_sl_19345
69.22 solcap_snp_sl_12856
70.73 solcap_snp_sl_14415
74.23 SL3.0ch12-64163939
82.37 SL3.0ch12-65137921
88.46 solcap_snp_sl_19630
95.17 SL3.0ch12-65948886
101.87 SL3.0ch12-67085895
105.00 solcap_snp_sl_6568
111.71 SL3.0ch12-65950521
111.71 SL3.0ch12-65950554
120.42 SL3.0ch12-65160241
Shin et al., 2020
Bwr12.1
Bwr12.2

817

818 Supplemental Figure 8: GBS Read Distribution by Sample (includes parental references).

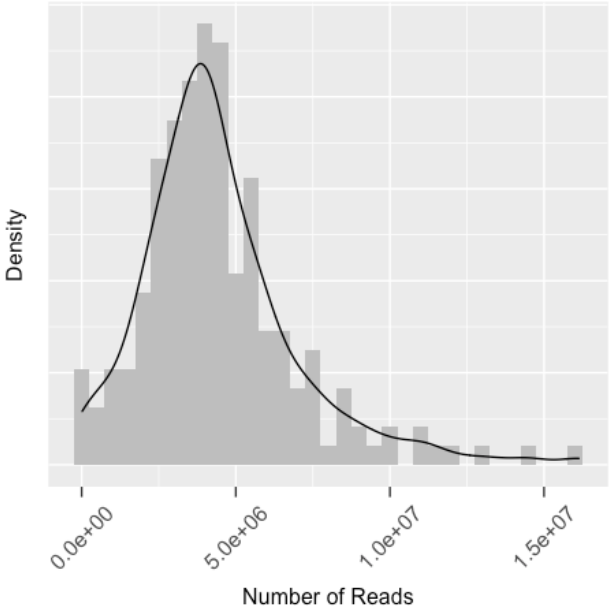

819
820
821
822
823
824
825
826
827
828
829
830
831
832
833
834
835
836
837
838

Supplemental Figure 9: a) RIL and parental coverage and SNP density from GBS analysis; b) Percent heterozygosity and SNP density

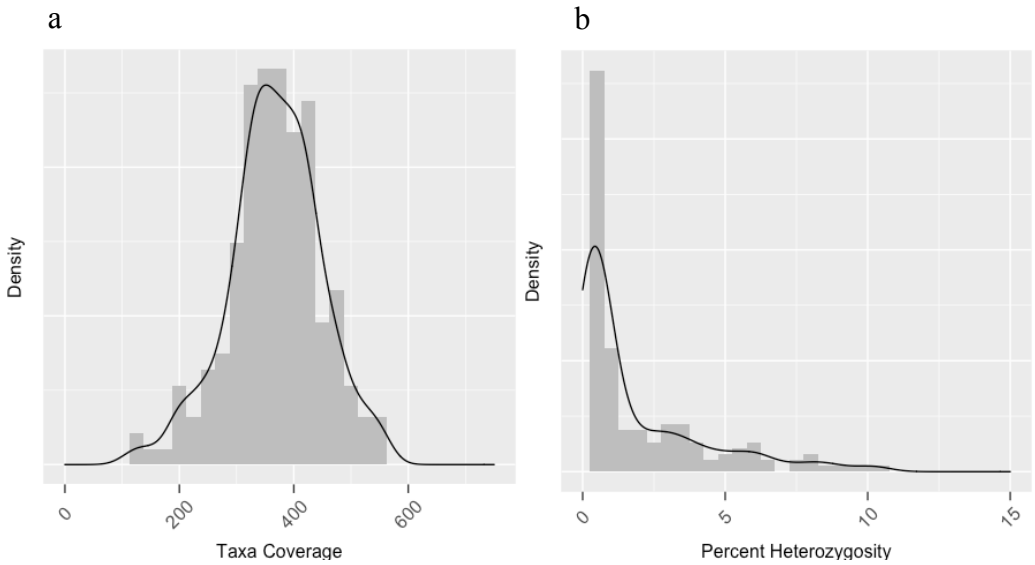

Supplemental Tables

Supplemental Table 1 Descriptive statistics for 10 image-based traits and two years of visually assessed wilting scores (2016 and 2019). Image-based traits were from the same plants as the visually assessed wilting score in 2019. The RIL population was inoculated with Ralstonia and visually scored for wilting in 2016, but images were not taken. Data is shown for resistant parent Hawaii 7996, susceptible parent West Virginia 700, and the RIL population.

		Hawaii 7996				West Virginia 700				RILs			
year	Variable	Mean	SD	Minimum	Maximum	Mean	SD	Minimum	Maximum	Mean	SD	Minimum	Maximum
2016	Wilting_Score	0	0	0	0	100	0	100	100	44.41	41.4	0	100
	Wilting_Score	0	0	0	0	99.33	5.16	60	100	53.69	42.23	0	100
	convex area	2.7e+06	1.4e+06	-4.1e+04	6.3e+06	-3.6e+05	3.6e+05	-1.1e+06	7.4e+05	1.2e+06	1.4e+06	-2.0e+06	7.9e+06
	convex width	8.7e+02	4.4e+02	-7.0e+01	1.7e+03	-7.4e+02	3.7e+02	-1.4e+03	5.4e+02	-4.6e-01	5.9e+02	-1.9e+03	2.9e+03
	plant area	8.7e+05	5.6e+05	-1.0e+04	2.2e+06	-1.1e+05	1.1e+05	-3.4e+05	2.1e+05	5.0e+05	5.5e+05	-7.4e+05	2.6e+06
	plant height	5.6e+02	1.9e+02	-7.0e+01	8.7e+02	-1.3e+01	1.7e+02	-3.6e+02	3.7e+02	3.3e+02	2.5e+02	-6.5e+02	1.1e+03
2019	plant width	4.0e+02	2.0e+02	-3.6e+01	8.2e+02	-3.5e+02	1.8e+02	-6.6e+02	2.5e+02	-2.1e+01	2.7e+02	-9.7e+02	8.4e+02
	X mass	3.1e+02	1.6e+02	-3.7e+01	5.8e+02	-2.9e+02	1.5e+02	-5.6e+02	2.0e+02	-1.2e+01	2.3e+02	-7.4e+02	6.9e+02
	Y mass	5.4e+02	2.1e+02	-8.4e+01	9.3e+02	-6.7e+01	1.6e+02	-4.1e+02	3.6e+02	2.1e+02	2.2e+02	-7.0e+02	9.6e+02
	CM width	3.1e+02	1.6e+02	-1.0e+02	6.0e+02	-2.9e+02	1.5e+02	-5.2e+02	1.8e+02	2.7e+01	2.3e+02	-7.0e+02	9.8e+02
	CM height	2.6e+02	1.8e+02	-2.1e+02	6.2e+02	-1.3e+02	1.5e+02	-3.9e+02	1.9e+02	-5.2e+01	1.9e+02	-8.8e+02	8.3e+02
	color average	2.88	5.44	-5.96	22.9	7.37	2.84	1.03	14.83	4.06	4.48	-11.35	16.48

882 Supplemental Table 2: Marker density per cM for each chromosome.

Chromosome	Number of marker	Chromosome Length (cM)	Average interval length (cM)	Standard deviation	Standard error
1	36	153.42	4.38	4.15	0.70
2	19	117.42	6.52	3.92	0.92
3	28	87.77	3.25	3.56	0.68
4	44	133.43	3.10	4.25	0.65
5	18	116.49	6.85	5.33	1.29
6	61	116.92	1.80	1.99	0.26
7	21	95.63	4.78	3.94	0.88
8	14	97.27	7.48	4.44	1.23
9	27	143.5	5.52	5.77	1.13
10	18	80.01	4.71	4.80	1.16
11	25	61.22	2.55	3.88	0.79
12	43	120.42	2.87	3.01	0.46

883
884
885
886
887
888
889
890
891
892
893
894
895
896
897
898
899
900
901
902
903
904

905 Supplemental Table 3: Overview of the 9 genomic regions identified with a LOD score greater
906 than 3 on chromosome 10 after inoculation with R. solanacearum at 6 dpi. According to the ICI
907 Mapping analysis using 1000 permutations, a threshold value of 3.48 represents the minimum
908 LOD to identify a significant QTL. Genomic regions with a lower LOD value did not reach our
909 threshold for significance after permutation.

Chromosome	Position	LeftMarker	RightMarker	TraitName	LOD	PVE	Add
10	51	solcap_snp_sl_33168	SL3.0ch10-63377492	Wilting Score 2019	3.0067	13.3810	0.2077
10	52	solcap_snp_sl_33168	SL3.0ch10-63377492	Wilting Score 2019	3.0927	10.5192	0.1842
10	53	solcap_snp_sl_33168	SL3.0ch10-63377492	Wilting Score 2019	3.0832	8.0396	0.1611
10	52	solcap_snp_sl_33168	SL3.0ch10-63377492	convex width	3.1634	9.0040	-0.1835
10	53	solcap_snp_sl_33168	SL3.0ch10-63377492	convex width	3.4883	7.8538	-0.1714
10	51	solcap_snp_sl_33168	SL3.0ch10-63377492	plant width	3.0398	11.1872	-0.2039
10	52	solcap_snp_sl_33168	SL3.0ch10-63377492	plant width	3.5411	10.2424	-0.1951
10	53	solcap_snp_sl_33168	SL3.0ch10-63377492	plant width	3.8661	8.8147	-0.1811
10	53	solcap_snp_sl_33168	SL3.0ch10-63377492	X mass	3.0584	7.0293	-0.1629

910
911
912
913
914
915
916
917
918
919
920
921
922
923
924
925
926
927
928

929 Supplemental Table 4: Overview of QTLs identified across the genome at all time points (-1, 3,
930 4, 5, 6 dpi) with R. solanacearum. LOD: maximum value of the Logarithm of the odd. PVE:
931 Percentage of phenotypic variance explained. Add: Additive effect, the positive and negative
932 values indicated that the alleles are introgressed from the resistant parent (Hawaii 7996) and
933 susceptible parents (WestVirginia). LeftCI and RightCI are the confidence interval calculated by
934 a one-LOD decrease from the estimated QTL position. * = Bwr3.1; ** = Bwr3.2
935

	Timepoint	Chromosome	Position	LeftMarker	RightMarker	TraitName	LOD	PVE	Add	LeftCI	RightCI
	-1	2	117	solcap_snp_sl_8510	solcap_snp_sl_15574	plant width	3.3851	6.4842	0.1290	114.5	117.0
	-1	2	117	solcap_snp_sl_8510	solcap_snp_sl_15574	X mass	4.1424	6.8279	0.1390	114.5	117.0
	-1	3	58	SL3.0ch03-61078160	solcap_snp_sl_10372	plant width	3.2538	9.4831	0.1555	56.5	64.5
	-1	3	58	SL3.0ch03-61078160	solcap_snp_sl_10372	X mass	3.8291	9.4218	0.1628	56.5	64.5
	-1	3	59	SL3.0ch03-61078160	solcap_snp_sl_10372	CM height	3.7940	3.6957	0.1603	56.5	63.5
	-1	3	30	solcap_snp_sl_9689	solcap_snp_sl_9681	plant area	3.6327	8.0934	0.1522	24.5	34.5
	-1	4	128	SL3.0ch04-1213025	solcap_snp_sl_63869	CM height	3.8063	12.0286	-0.2891	127.5	130.5
	-1	6	10	SL3.0ch06-13533085	SL3.0ch06-3310762	convex area	4.7410	11.2755	0.1621	8.5	11.5
	-1	6	10	SL3.0ch06-13533085	SL3.0ch06-3310762	plant width	3.5865	6.9265	0.1336	8.5	11.5
	-1	6	10	SL3.0ch06-13533085	SL3.0ch06-3310762	plant area	3.5117	7.3344	0.1457	8.5	11.5
	-1	6	10	SL3.0ch06-13533085	SL3.0ch06-3310762	X mass	4.8686	8.0160	0.1510	8.5	11.5
	-1	6	10	SL3.0ch06-13533085	SL3.0ch06-3310762	Y mass	4.9020	9.3612	0.1757	8.5	11.5
	-1	8	80	solcap_snp_sl_21461	SL3.0ch08-63373341	X mass	3.2439	5.3622	0.1230	74.5	83.5
	-1	9	67	SL3.0ch09-39293163	SL3.0ch09-63338944	convex area	3.1976	7.5230	-0.1323	60.5	69.5
	-1	9	36	solcap_snp_sl_26683	SL3.0ch09-4516570	CM height	4.8307	6.1460	0.2081	32.5	40.5
	-1	10	71	solcap_snp_sl_8835	Le013158s_161	Y mass	3.2077	5.9734	0.1404	68.5	73.5
*	3	3	25	solcap_snp_sl_14355	solcap_snp_sl_9689	CM height	7.2477	18.2665	0.2584	21.5	30.5
	3	3	27	solcap_snp_sl_14355	solcap_snp_sl_9689	CM width	3.5022	8.8528	0.1536	22.5	32.5
	3	3	26	solcap_snp_sl_14355	solcap_snp_sl_9689	plant width	5.5180	13.9255	0.2191	21.5	27.5
**	3	3	26	solcap_snp_sl_14355	solcap_snp_sl_9689	X mass	4.5407	11.7470	0.1991	22.5	32.5
	3	3	39	solcap_snp_sl_21215	solcap_snp_sl_9663	convex width	5.6025	13.8198	0.2120	37.5	42.5
	3	3	28	solcap_snp_sl_9689	solcap_snp_sl_9681	plant height	4.5094	10.3345	0.1974	25.5	31.5
	3	3	28	solcap_snp_sl_9689	solcap_snp_sl_9681	Y mass	5.7227	15.0239	0.2325	23.5	31.5
**	4	3	39	solcap_snp_sl_21215	solcap_snp_sl_9663	convex width	3.9750	10.2036	0.1829	37.5	43.5
	4	3	39	solcap_snp_sl_21215	solcap_snp_sl_9663	CM width	4.5294	8.4260	0.1853	37.5	43.5
	4	3	39	solcap_snp_sl_21215	solcap_snp_sl_9663	plant width	3.8768	9.9017	0.1838	37.5	43.5
	4	3	39	solcap_snp_sl_21215	solcap_snp_sl_9663	X mass	3.8156	9.7282	0.1837	37.5	43.5
	4	3	28	solcap_snp_sl_9689	solcap_snp_sl_9681	convex area	3.1310	7.7809	0.1508	22.5	32.5
	4	3	30	solcap_snp_sl_9689	solcap_snp_sl_9681	plant area	3.8685	9.9594	0.1672	23.5	33.5
*	5	3	22	solcap_snp_sl_14355	solcap_snp_sl_9689	CM height	3.6770	9.3886	0.1414	21.5	27.5
	5	3	22	solcap_snp_sl_14355	solcap_snp_sl_9689	plant width	3.4953	9.3017	0.1806	21.5	27.5
	5	3	25	solcap_snp_sl_14355	solcap_snp_sl_9689	plant height	3.6851	8.5381	0.1738	21.5	31.5
	5	3	25	solcap_snp_sl_14355	solcap_snp_sl_9689	Y mass	3.4687	9.9830	0.1673	21.5	31.5
**	5	3	39	solcap_snp_sl_21215	solcap_snp_sl_9663	convex width	3.7859	9.8306	0.1891	37.5	43.5
	5	3	39	solcap_snp_sl_21215	solcap_snp_sl_9663	CM width	4.0630	7.4955	0.1924	35.5	39.5
	5	5	107	SL3.0ch05-65105663	SL3.0ch05-66111590	plant height	3.4091	8.9327	0.1778	104.5	114.5
	5	12	56	SL3.0ch12-62154155	solcap_snp_sl_19345	CM height	3.2828	8.2102	0.1360	54.5	59.5
	6	2	72	SL3.0ch02-45885016	SL3.0ch02-44375028	X mass	3.4765	9.4924	-0.2178	69.5	73.5
	6	2	72	SL3.0ch02-45885016	SL3.0ch02-44375028	CM width	3.2455	8.4550	-0.2189	69.5	73.5
	6	2	45	solcap_snp_sl_18519	SL3.0ch02-49265134	plant width	3.4108	6.4576	-0.1669	42.5	47.5
*	6	3	22	solcap_snp_sl_14355	solcap_snp_sl_9689	convex width	5.3238	10.2506	0.2103	21.5	26.5
	6	3	22	solcap_snp_sl_14355	solcap_snp_sl_9689	plant width	4.7309	9.1511	0.1976	21.5	25.5
	6	3	25	solcap_snp_sl_14355	solcap_snp_sl_9689	plant height	4.5107	7.6902	0.1896	21.5	31.5
	6	3	23	solcap_snp_sl_14355	solcap_snp_sl_9689	CM width	3.6627	6.2716	0.1887	21.5	27.5
	6	3	22	solcap_snp_sl_14355	solcap_snp_sl_9689	X mass	3.4765	5.8012	0.1705	21.5	26.5
	6	3	25	solcap_snp_sl_14355	solcap_snp_sl_9689	Y mass	3.3918	9.3283	0.1708	21.5	31.5
**	6	3	38	solcap_snp_sl_21215	solcap_snp_sl_9663	Wilting Score 2016	3.5258	7.3736	-0.1726	35.5	39.5
	6	3	38	solcap_snp_sl_21215	solcap_snp_sl_9663	convex area	3.4328	9.0796	0.1953	34.5	39.5
	6	3	38	solcap_snp_sl_21215	solcap_snp_sl_9663	plant area	3.3019	8.6697	0.1902	34.5	39.5
	6	4	4	SL3.0ch04-60431371	solcap_snp_sl_11543	convex width	3.1855	6.0199	0.1627	1.5	10.5
	6	5	100	solcap_snp_sl_22649	SL3.0ch05-65105663	plant height	3.6115	9.4852	0.2103	95.5	103.5
	6	6	79	solcap_snp_sl_14458	SL3.0ch06-39435402	Wilting Score 2016	4.0770	8.7626	-0.1871	76.5	81.5
	6	6	81	solcap_snp_sl_14458	SL3.0ch06-39435402	Wilting Score 2019	3.2673	11.0473	-0.1621	78.5	81.5
	6	10	53	solcap_snp_sl_33168	SL3.0ch10-63377492	plant width	3.8661	7.6897	-0.1811	50.5	54.5
	6	10	53	solcap_snp_sl_33168	SL3.0ch10-63377492	convex width	3.4883	6.8155	-0.1714	50.5	54.5
	6	12	37	solcap_snp_sl_1525	solcap_snp_sl_1572	CM height	4.1755	10.7222	0.1837	33.5	40.5
	6	12	42	solcap_snp_sl_58807	solcap_snp_sl_9707	Y mass	3.3249	8.5939	0.1651	40.5	43.5

937